Title
Spatio-mechanical EphA2/ephrin-A1 Signaling in Cancer Cells

Author
Xu, Qian

Publication Date
2011

Peer reviewed|Thesis/dissertation

Spatio-mechanical EphA2/ephrin-A1 Signaling in Cancer Cells

by

Qian Xu

A dissertation submitted in partial satisfaction of the

requirements for the degree of

Doctor of Philosophy

in

Biophysics

in the

Graduate Division

of the

University of California, Berkeley

Committee in charge:

Professor Jay T. Groves, Chair
Professor John Kuriyan
Professor Jan Liphardt
Professor Kunxin Luo

Spring 2011

Spatio-mechanical EphA2/ephrin-A1 Signaling in Cancer Cells

By

Qian Xu

Abstract

Spatio-mechanical EphA2/ephrin-A1 Signaling in Cancer Cells

by

Qian Xu

Doctor of Philosophy in Biophysics
University of California, Berkeley
Professor Jay T. Groves, Chair

Communication strategies in nature are an integral part to the survival of multi-cellular organisms. Cell membranes provide the chemical environment in which intercellular signaling begins. The vast complexity of this signaling requires that a relatively conserved set of chemical constituents be able to generate enormous signal diversity. Spatial sorting of signaling molecules within the membrane allows for this diversity. My research uses synthetic lipid membranes, solid-state nanostructures, and high-resolution imaging to study a potentially novel spatio-mechanical regulatory mechanism in the EphA2 signaling pathway. My hypothesis is that the multi-scale organization of the EphA2 receptor in the cell membrane regulates its biochemical function. This hypothesis is motivated by the idea that extracellular mechanical inputs have an important role in intracellular signaling cascades.

Acknowledgements

The journey that would eventually take me to this moment in time started when I purchased a copy of *In Search of Schrödinger's Cat* by John Gribbin at the local mall on an leisurely outing with my friends in high school. I became fascinated with not just particle physics but also physicists, falling in love with the likes of Richard Feynman, Paul Dirac, and even a brief fling with Don Glaser, whom I met later in my life, in person. I was on a completely different course then and he, as I heard him say, had decided that since he already has a Nobel Prize in physics, he would go into biology. And that's where I ended up, in biophysics.

The span of this journey and the process of solidifying my ideas are the result of having both supporters as well as opponents in my life. I thank them here.

First, I want to thank my parents for not supporting my life decisions. This is crucial because if it hadn't been for their discouragements and criticisms of my choices (which was on anything that was not going to medical school and becoming a doctor), I would never have given serious thought to my choices. The chance to defend your decisions in the face of strong opponents is the best way to ensure success, after you have succeeded in your arguments with yourself. It was in these struggles that I learned, the hard way, how to figure things out.

Second, I would like to thank my high school friend, Emily Wright, for encouraging my passions, even without understanding them which was exactly what I had wished my parents would do. At that time, I told her that I would become a "4-dimensional quantum biopsychological physicist". Without questioning the meaning of that title, the next holiday, she gave me *Time Travel Through Einstein's Universe* by J. Richard Gott. She had given me her support and that was all I needed to figure things out.

Third, I would like to thank Jim Sellers and Fei Wang for introducing me to scientific research and giving me the opportunity to work in an research environment that set the stage for my future research related endeavors. It was in this environment that I started to appreciate the modest scientific problems that can be realistic approached at the bench-research level.

Lastly, I want to thank everyone in my present life, my current and past co-workers Pradeep Nair, Mike Coyle, Niña Hartman, Lia Ball, Hector Huang, Wan-Chen Lin, Sara Triffo, Rebecca Petit, Theo Lohmüller, and Jay Groves. You guys make everyday go by so much faster and help me figure out science through wonderful discussions both realistic and philosophical in nature. Jay, thank you for being an extremely effective advisor in ways that will forever remain a mystery to me.

Brian, you already know what I have to say. I dedicate this thesis to you. You have helped me figure many things out.

And this takes me back to the beginning, to Feynman, who taught me the *pleasure* of figuring things out. Thank you.

Chapter 1

EphA2/ephrin-A1 Signaling in Cancer

"Piled Higher and Deeper" by Jorge Cham, www.phdcomics.com

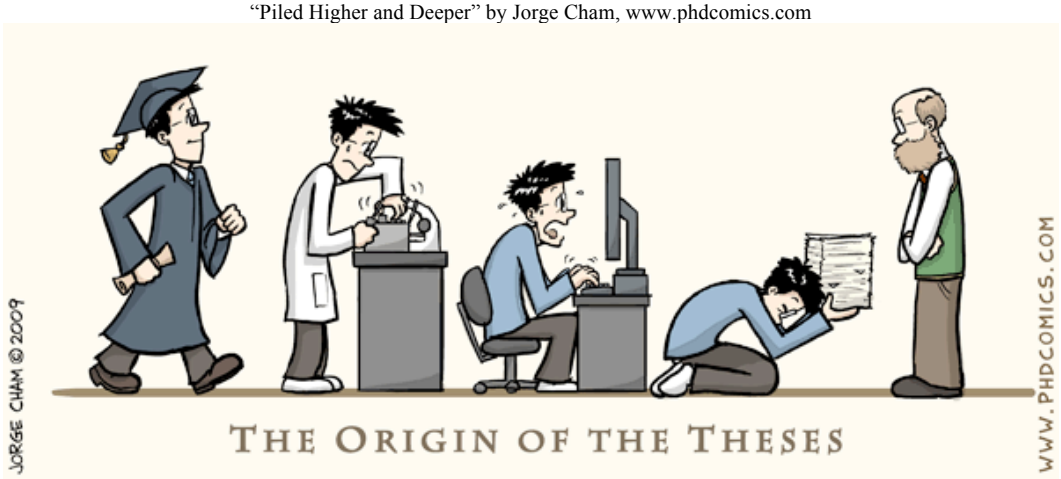

1.1 CANCER METASTASIS

Metastasis, the spread of malignant tumor cells from a primary tumor to different locations, is responsible for over 90% of all cancer patient fatalities[1]. Associated with this are a number of open questions, most important of which is why some tumor cells are more likely to invade surrounding tissue and metastasize than others. The answer is likely found within individual cells rather than the tumor population because although millions of cells are constantly released from the tumor into circulation in the body, only a tiny minority will initiate colonization at distant organ sites[1]. Genetic mutations and protein overexpressions are often used to predict the likelihood of tumor formation [2]. However, these properties cannot distinguish between the invasion potential of one tumor cell from another chemically similar tumor cell. Physical properties of the microenvironment surrounding the tumor cells such as interstitial pressure and tensional force, in cooperation with the intrinsic biochemistry of the cells, have been illustrated to promote proliferation and progression [3]. Furthermore, membrane bound receptor tyrosine kinases (RTK) are identified as initiators of cancer cell invasion and metastasis because they are capable of both sensing the extracellular environment as well as communicating with intracellular molecules [4].

1.2 EPHA2 SIGNALING

Eph receptor tyrosine kinases, through binding to either glycosylphophatidylinositol (GPI)-linked or transmembrane ephrin ligands, are important regulators of cell adhesion, migration, and vascular development [5]. Eph and ephrin interactions have been shown to both suppress and promote cancer formation by altering cell repulsion and migration [6]. In particular, EphA2 and its GPI-linked ligand ephrin-A1 are important in maintaining many different tumor types [7]. Overexpression of EphA2 in nontransformed mammary epithelial cells confers malignant transformation and tumorigenic potential [8]. Decreasing expression of EphA2 can reverse metastatic behavior in immortal breast epithelial cell lines [9]. In addition to these pro-ocogenic properties of overexpressed EphA2, this receptor has also been shown to suppress tumorigenesis. For example, EphA2 knockout mice are more susceptible to develop skin cancer upon exposure to known carcinogens [10]. These findings, among others, have led EphA2 to become a target for cancer therapeutics.

EphA2 consists primarily of an intracellular kinase domain, an extracellular ligand-binding domain, and a transmembrane domain [11]. Activation of EphA2 is marked by phosphorylation of the kinase domain [12] and can lead to receptor internalization and degradation through the recruitment of metalloproteases to the cell membrane [13]. Ligand-induced receptor activation occurs upon the binding of EphA2 to its ephrin-A1 ligand presented on apposed cell membranes. Ligand binding is generally followed by dimerization of the receptor-ligand complex, oligomerization as a result of three distinct ligand binding sites on the receptor [14], and possibly larger scale cell surface reorganization [15]. The clustering and subsequent endocytosis of EphA2 has been hypothesized as a method of regulating cell surface EphA2 levels [16]. Ligand-induced receptor clustering has been proposed as a likely source of signal regulation that is independent of any conformational changes within the receptor and therefore a potential deregulatory

mechanism in Eph-overexpressing tumors [17].

1.3 LIVE CELL – SUPPORTED MEMBRANE PLATFORM

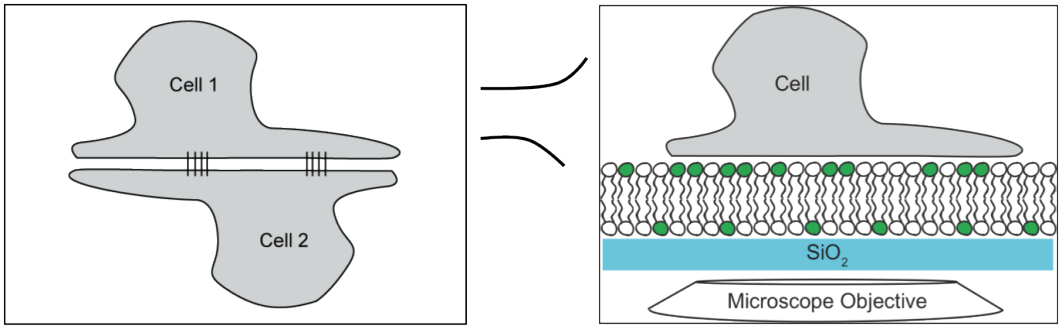

Figure 1.1. The live cell – supported membrane interface recapitulates the juxtacrine signaling interface between two live cells *in vivo*.

The hybrid live cell — supported lipid bilayer (SLB) junction (Fig. 1.1), in which one cell surface in a juxtacrine signaling process is replaced by a SLB displaying ligands of interest, has proven to be an effective strategy to examine cell-cell signaling [15,18,19]. SLBs can be formed by the spontaneous self-assembly of a phospholipid bilayer upon deposition of vesicles onto a silica support [20]. The resulting membrane is continuous and fluid, with lipid lateral mobilities typically ranging from 1 – 3 $\mu m^2/s$ [21]. GPI-linked proteins can be incorporated into SLBs without loss of mobility [22]. In many cases, including the work presented here, protein linkage to the membrane by multivalent interactions between decahistidine tails on the protein and Ni-chelating lipids in the membrane is equally effective [23], and technically much simpler [24]. We have recently used the live cell – SLB junction, functionalized with a preclustered EA1 ligand, to study properties of EphA2 signaling [15]. This work revealed that the EphA2 signaling pathway is sensitive to the physical restriction of receptor-ligand movement over micron length-scales within the plane of the cell-SLB interface. These results raise interesting hypotheses concerning the possibility of mechanosensing in relation to EphA2 signaling and they also underscore the importance of large-scale receptor assembly as a regulatory component of signaling. In this regard, however, the use of preclustered ligands is especially problematic since it essentially bypasses natural receptor assembly processes.

Chapter 2

EphA2 Receptor Activation by Monomeric Ephrin-A1 on Supported Membranes

"Piled Higher and Deeper" by Jorge Cham, www.phdcomics.com

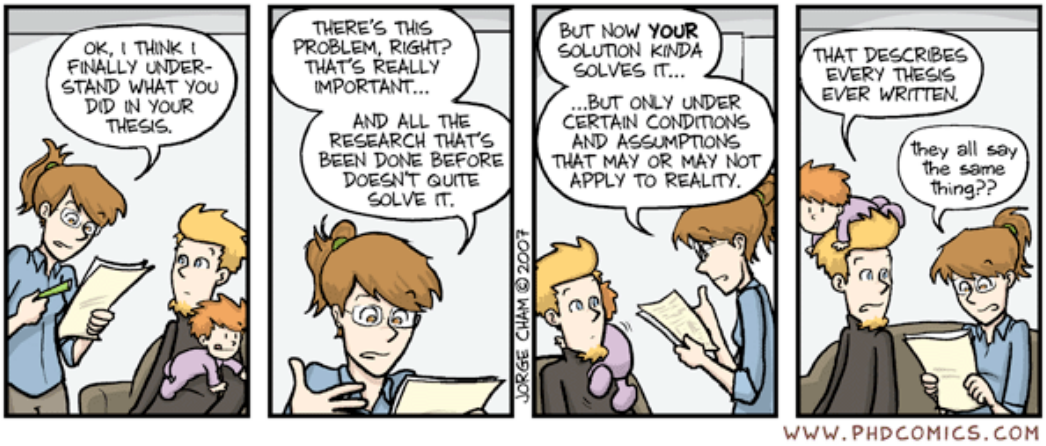

2.1 ABSTRACT

The receptor tyrosine kinase EphA2 interacts with its GPI-linked ephrin-A1 ligand in a juxtacrine configuration. The soluble ephrin-A1 protein, without its GPI membrane linker, fails to activate EphA2. However, preclustered ephrin-A1 protein is active in solution and has been frequently used to trigger the EphA2 receptor. While this approach has yielded insights into EphA2 signaling, preclustered ligands bypass natural receptor clustering processes and thus mask any role of clustering as a signal regulatory mechanism. Here we present EphA2-expressing cells with a fusion protein of monomeric ephrin-A1 (mEA1) and enhanced monomeric yellow fluorescent protein that is linked to a supported lipid bilayer (SLB) via a nickel-decahistidine anchor. The mEA1 is homogeneously dispersed, laterally mobile, and monomeric as measured by fluorescence imaging, correlation spectroscopy, and photon counting histogram analysis, respectively. Ephrin-A1 presented in this manner activates EphA2 on the surface of MDA-MB-231 human breast cancer cells, as measured by EphA2 phosphorylation and degradation. Spatial mutation experiments in which nanopatterns on the underlying substrate restrict mEA1 movement in the SLB reveal spatio-mechanical regulation of this signaling pathway, consistent with recently reported observations using a synthetically crosslinked ephrin-A1 dimer.

2.2 INTRODUCTION

Eph receptors bind to ephrin ligands as a 1:1 complex [25] and can be activated by ephrin expressed on cell membranes or in a preclustered format [26]. Soluble monomeric ephrin has generally been considered inactive. However, a recent report suggests that the media containing soluble and monomeric ephrin-A1, released from tumor cells, through possible cleavage processes, is capable of activating EphA2 in paracrine signaling [27]. These contradictory findings underscore the complexity of Eph/ephrin interactions. Based on prior observations of inactive monomeric protein ligands becoming active in juxtacrine signaling from supported membranes, for example major histocompatibility complex in T cell receptor signaling [28] and neuroligin in neurexin signaling [29], we hypothesized that laterally mobile and monomeric ephrin-A1 presented on a supported membrane may activate the EphA2 receptor in the absence of synthetic cross-linking agents. Furthermore, this platform will provide a useful tool to study the signaling pathway and the effects of natural ligand clustering processes.

We constructed a fusion protein of monomeric ephrin-A1 (mEA1), enhanced yellow fluorescent protein (EYFP), and a 10-histidine (H10) tail. We have previously shown that H10 tails can form essentially irreversible multivalent linkage with Ni-chelating lipids in SLBs when assembled using kinetically controlled parameters [24]. Fluorescence imaging of the mEA1-EYFP-H10 fusion protein in SLBs reveals that it is homogeneously distributed. Fluorescence correlation spectroscopy confirms that it is laterally mobile with a diffusion coefficient similar to that of the lipids and photon counting histogram analysis reveals the protein to be predominantly monomeric on the membrane surface. The supported membrane-associated mEA1 activates the EphA2 receptor signaling pathway in live EphA2-expressing human breast cancer cells (MDA-MB-231), as measured by receptor phosphorylation and degradation. The soluble mEA1 is

inactive in these experiments. Additionally, spatial mutation experiments in which nanopatterned structures on the underlying substrate are used to manipulate the movement and assembly of receptor-ligand complexes reveal spatio-mechanical influences over the EphA2 signaling pathway similar to recently reported observations using a synthetically crosslinked ephrin-A1 dimer, EA1-Fc [15]. Large-scale EphA2/ephrin-A1 assembly occurs during activation even without any preclustering of the ligand and mechanical interference with this process leads to distinct alterations in cell behavior, as observed by cytoskeleton morphology and recruitment of the metalloprotease, ADAM10.

2.3 RESULTS and DISCUSSION

2.3.1 EA1 association with supported membranes is stable and properly oriented

The EA1 fusion protein is expressed by combining the human monomeric EA1 ectodomain sequence, along with the EYFP sequence, with an H10 tail on the C-terminus for linkage to Ni-chelating lipids, which are incorporated into the supported membrane at molar ratios ranging from 0.005 to 0.06 (Fig. 2.1A).

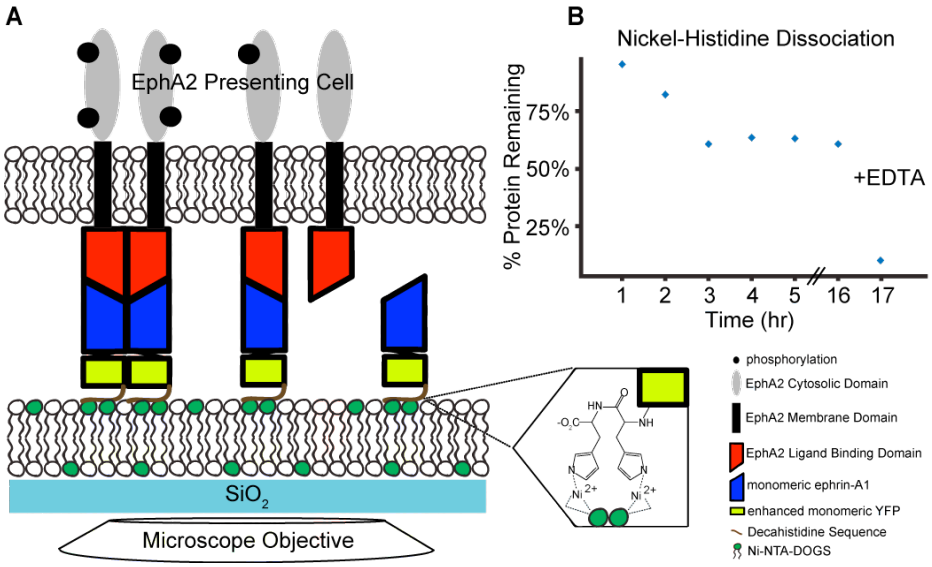

Figure 2.1. Schematic diagram of the experimental set-up. **A)** EphA2-expressing breast cancer cells are cultured on a SLB consisting of a tunable surface density of EA1 fusion proteins. This fusion protein is designed by linking the soluble portion of monomeric human ephrin-A1 with enhanced YFP that has an A206K mutation to prevent dimer formation. The inset shows the anchoring strategy which is stable when the decahistidine sequence at the C-terminus of the fusion protein is chelating multiple Nickel ions that are chelated by a tunable subset of lipids within the bilayer. **B)** Nickel-histidine dissociation curve shows that protein binding reaches a kinetically trapped state (plateau in graph between 3 and 16 hours) that is stable and therefore insensitive to rinsing steps well beyond the time scale of experiments. The bilayer is incubated at 25°C for the entirety of the measurements except for an hour at 37°C after the first 2 hours. The high temperature incubation period is performed to mimic the period after cells are introduced and then incubated at 37°C for an hour.

Multivalent Ni-histidine interactions are necessary to stably associate protein through this method (Fig. 2.1A inset) [24]. Typically, protein is incubated under carefully tuned kinetically controlled parameters to optimize for mutlivalent interactions. It is also generally necessary to allow a desorption period to remove weakly associated protein. A Ni-histidine dissociation curve is generated to show that the mutlivalent Ni bound protein remains stably bound to the SLB for at least 16 hours on a SLB (Fig. 2.1B). The protein linkage through histidine – chelated Ni

interactions is confirmed by the addition of 100mM Ethylenediaminetetraacetic acid (EDTA), which strongly sequesters metal ions and leads to dissociation of protein bound in this manner (Fig. 2.1B).

2.3.2 EA1 is mobile and predominantly monomeric in supported membranes

Fluorescence correlation spectroscopy (FCS) along with its counterpart photon counting histogram (PCH) analysis offer a powerful means to quantify the lateral mobility and the cluster size distribution of EA1 on the SLB surface [30]. A typical time autocorrelation function of fluorescence intensity fluctuations from membrane bound EA1 is plotted in Figure 2.2A. The data is fitted to an analytical expression of normal 2-dimensional diffusion in a 2-dimensional Gaussian illumination spot,

$$G(\tau) = \frac{1}{N_{ave}} * \frac{1}{1 + \frac{\tau}{\tau_D}} \quad (1)$$

where N_{ave} represents the average number of independent molecules, τ is the time interval, and τ_D represents the characteristic residence time [31].

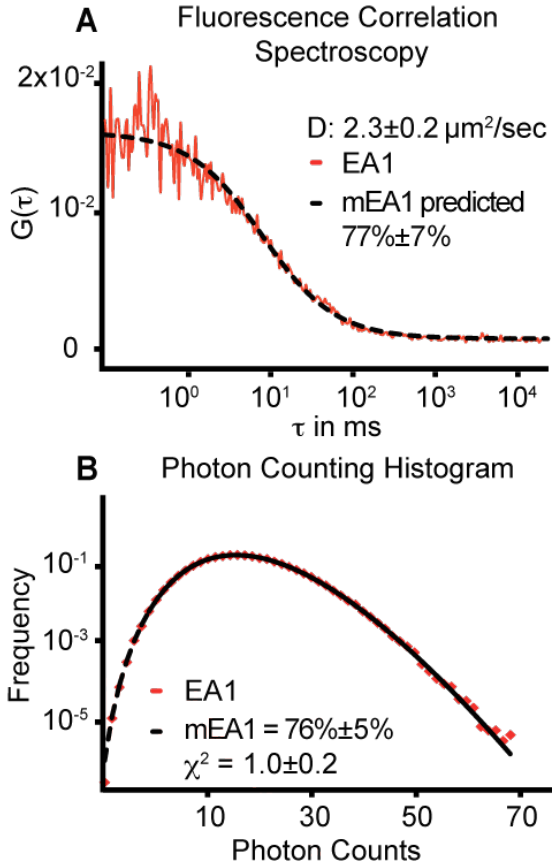

Figure 2.2. Characterization of mEA1 – SLB surface heterogeneity and protein cluster size. **A)** Fluorescence correlation spectroscopy (FCS) is used to determine the heterogeneity of the surface. Values are fitted to a standard 2-dimensional, single component curve. The diffusion constant calculated for the majority species is comparable to protein diffusion constants on cell membranes *in vivo*. A derivation of the autocorrelation function is used to relate the fraction of monomer to the average aggregation number (Q). From 2 independent FCS experiments, the derived function predicts that the fraction of monomeric species is 77%±7% for a Q value of 3. **B)** The photon counting histogram (PCH) is best fit by a two species fit. The majority of

the surface protein molecules (76%±5%) exhibit an average fluorescence intensity corresponding a single EYFP flourophore, indicating that the majority of the species exists as monomer fusion proteins. This percentage is an average across 3 independent PCH experiments.

Based on this model, the calculated diffusion coefficient for membrane EA1 is 2.3±0.2μm^2/s. This value is typical for lipid diffusion in supported membranes [32] and also consistent with fluorescence recovery after photobleaching (FRAP) experiments (Fig. 2.3).

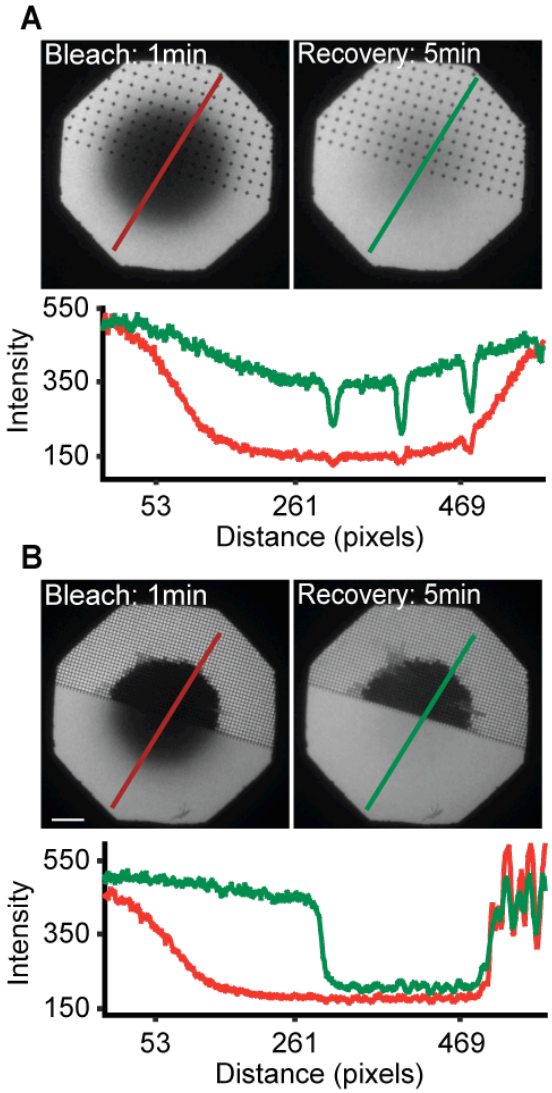

Figure 2.3. Fluorescence recovery after photobleaching is performed on mEA1 supported membranes. The fluidity of the mEA1 surface is verified through FRAP measurements for two different types of Cr patterns: **A**) crosses and **B**) 1micron pitches. These measurements show that the EA1-YFP SLB surface is fluid across micron length scales. Bar is 10μm.

Although tempting, one should not infer from this observation that the protein is monomeric. In order for FCS to resolve two components by their diffusion coefficients, a significant and well defined difference in mobility is necessary [33]. Since the EA1 is anchored to the membrane, its mobility is dominated by the membrane [34]. As such, there is no well-defined scaling of molecular mobility with size and furthermore, the effective size of dimers, trimers, etc., is not at all clear [35]. In light of these complexities, molecular mobility is an unreliable indicator of molecular size or

state of clustering.

Direct analysis of the distribution of photon arrival times (PCH) emitted by the EYFP molecules (that are genetically fused to EA1) diffusing through the open confocal spot provides a significantly more sound method of determining the aggregation state of EA1 (Fig. 2.2B). The fluorescence intensity fluctuations caused by the EYFP molecules yield a super-Poisson (Poi) distribution of photon counts arriving at the detector for a given time interval [36]. By choosing a time interval that is short relative to the timescale for molecules to move through the laser spot, the PCH reflects the cluster size distribution and, importantly, is independent of mobility. The probability distribution of a single molecule, $p^{(1)}$, diffusing within a closed system, V_0, is expressed as,

$$p^{(1)}(k;V_0,\varepsilon) = \int Poi(k,\varepsilon\overline{PSF}(\vec{r}))p(\vec{r})d\vec{r} \tag{2}$$

where $\overline{PSF}$ is the scaled point spread function for synchronizing the PCH volume with the FCS volume, $p(\vec{r})$ represents the probability to find the molecule at position $\vec{r}$, k is the detected photon count, and ε is the molecular brightness of the molecule. For N independent and identical molecules, the joint probability distribution $p^{(N)}$ is calculated from consecutive convolutions of $p^{(1)}$. It is expressed as,

$$p^{(N)}(k;V_0,\varepsilon) = (p_1^{(1)} \otimes ... \otimes p_N^{(1)})(k;V_0,\varepsilon) \tag{3}$$

It is numerically easier and equally accurate to select a reference volume (V_1) that is smaller than the reservoir (V_0) for deriving the PCH probability distribution so that the N value can remain small [36]. The probability distribution for multiple molecules in an open system is the expectation value of $p^{(N)}$, which is weighted by the Poissonian probability, $p_{\#}(N)$, of observing N particles,

$$\prod(k;\overline{N}_{PSF},\varepsilon) \equiv \hat{p}(k;V_1,\overline{N},\varepsilon) = \left\langle p^{(N)}(k;V_1,\varepsilon)\right\rangle_N = \sum_{N=0}^{\infty} p^{(N)}(k;V_1,\varepsilon)p_{\#}(N) \tag{4}$$

where the change from $\overline{N}$ to $\overline{N}_{PSF}$ reflects the selection of a V_1 that is smaller than V_0. This change does not affect the photon count probability because this probability of an open system is independent of the volume V_1 as long as this probability can be referenced to the concentration of the molecule [36]. In the case of membrane EA1, an accurate independent measurement of the surface density of EA1 is required to determine the N. This is achieved using quantitative fluorescence (QF) microscopy which calibrates fluorescence from the membrane-bound analyte with fluorescent lipid standards with known membrane surface densities [37]. Once this value is determined through QF, it is inserted into Eq. 4 and the resulting probability distribution is used to fit the membrane EA1 PCH. Since the PCH analysis has been experimentally demonstrated to be capable of resolving the aggregation state of fluorescent proteins [38], given an accurate value of N, both the average aggregation state (Q) and fraction (F) of monomeric EA1 can be determined from the best fit probability distribution, which has a local χ^2 value closest to 1. Interestingly, the relationship between Q and F can be separately derived from the $G(0)$ of the autocorrelation function for a two-component model as,

$$G(0) = \frac{Q + F(1-Q)}{N} \tag{5}$$

where N is determined by QF measurements and $G(0)$ is calculated from Eq.1 as $\frac{1}{N_{ave}}$ (see Section 2.5.9 for derivation). Therefore, for a given integral value of Q , the F value can be predicted by Eq. 5.

Using lipid bilayer standards with known surface densities, we can directly characterize the precision with which both FCS and PCH can determine the surface density (Fig. 2.4A-B). Using lipid bilayers with boron-dipyrromethene(Bodipy) fluorescent dyes attached to the headgroups of phospholipid molecules, incorporated into the bilayer at molar ratios, 0.0001, 0.0002, and 0.0004, FCS and PCH results are in precise agreement with each other as well as the known surface densities (Fig. 2.4C-D).

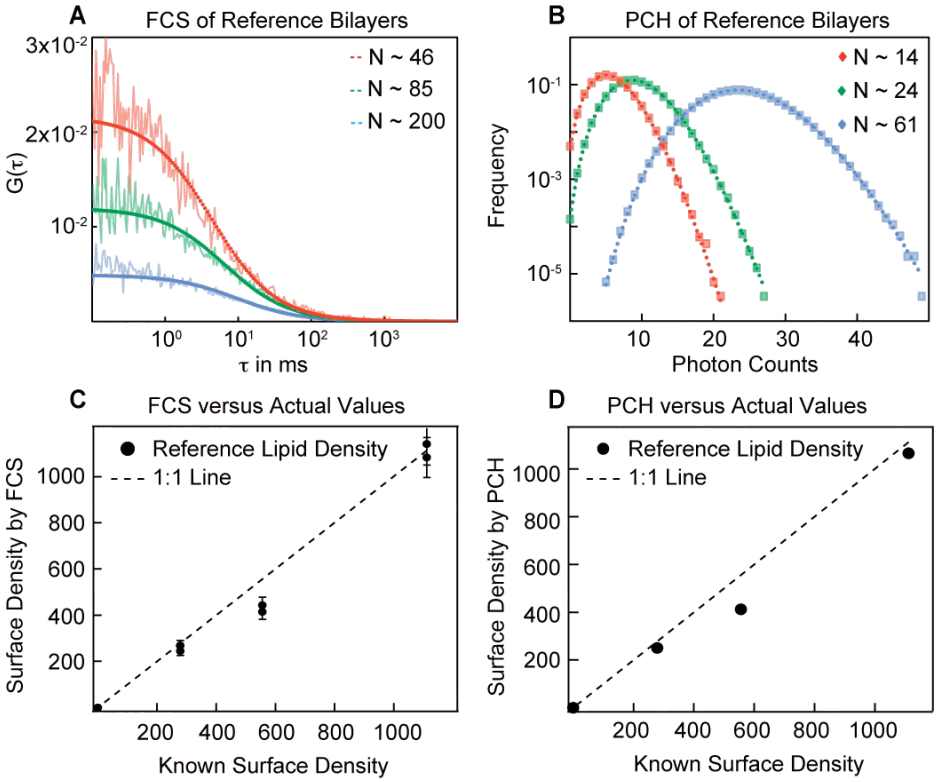

Figure 2.4. Surface density determination compared across fluorescence correlation spectroscopy and photon counting histogram. FCS **A)** and PCH **B)** are performed on reference lipid bilayers with increasing fluorophore lipid mole percent. The measurements and subsequent calculations are performed with the assumption that the lipid fluorophores are monomeric and the knowledge that the probability distribution of photon counts of an open system is independent of the reference volume and can be linearly rescaled to determine the surface density in terms of molecules/μm^2 [36]. After this rescaling, the surface densities determined by FCS **C)** and PCH **D)** are compared to known lipid surface densities assuming each lipid headgroup occupies a footprint of $0.72nm^2$ [39].

For these standards, the fluorescent lipid molecules are expected to move as monomers, in which case N is simply the number of molecules. Using these three standard lipid membranes, QF is performed to determine the surface density of membrane EA1. Calibration of spectral properties between the YFP fluorophore on EA1 and the lipid standard is performed in solution to obtain a scaling factor [37] of 0.7 (Fig. 2.5A). This relationship is linear at unsaturated fluorophore concentrations [37], enabling direct extrapolation to determine the EA1 surface density from measured fluorescence intensity (Fig. 2.5B). When N determined from surface density measurements by QF is used to interpret the two species autocorrelation function (Eq. 5), 77%±7% of EA1 is found to be monomeric (mEA1) and the remaining 13% has a Q value of 3 (trimers). Similarly, the best probability distribution fit to the PCH data is a two species curve resulting in an average local χ^2 of 1.0±0.2, corresponding to 76%±5% mEA1 with Q also equal

to 3.

In order to gauge the precision of this methodology to determine clustering state, probability distributions are also calculated for cases of several different aggregation states: solely monomeric, dimeric, or trimeric EA1. The respective residuals are plotted in Figure 2.6. The resolution of PCH in distinguishing between aggregation states can be revealed in the poor χ^2 values of these cases. We conclude from two independent methods that the membrane-associated EA1 is predominantly monomeric.

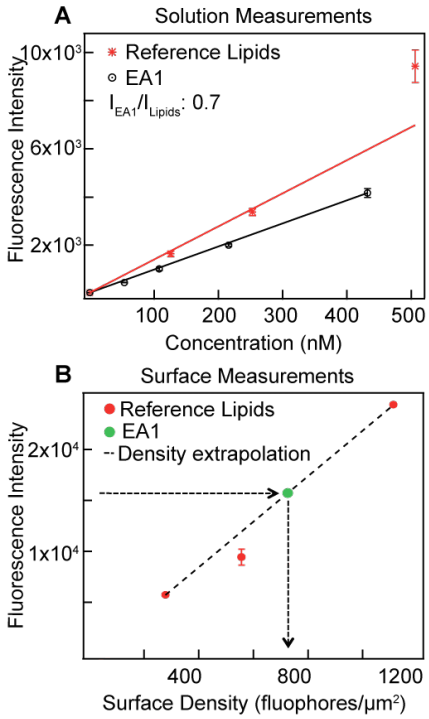

Figure 2.5. Quantitative fluorescence analysis to determine EA1 surface density on SLB. The protein is compared to a lipid standard, Bodipy FL DPHE. The solution concentrations of the lipid vesicles and protein are titrated and then measured to determine the respective fluorescence intensities, which has been previously shown to scale linearly with the concentration [37]. The scaling factor between the Bodipy fluorophore of the reference lipid and the EYFP portion of the EA1 fusion protein is calculated from the slopes of graphs in **A)** and factored into the slope of graph in **B)** to extrapolate the surface density of the protein given a measured fluorescence intensity value.

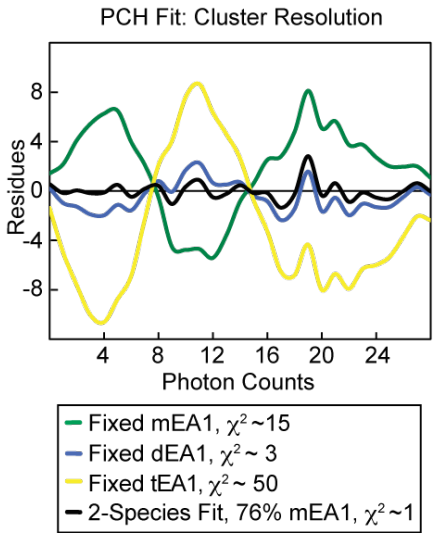

Figure 2.6. Resolving cluster states with PCH. The surface density of mEA1-YFP fluorophores is measured by QF which is used to fix the *N*, representing the number of monomer molecules in the probability distribution fit of the PCH data. Using this fixed *N*, the probability distributions for 3 different cases are calculated by assuming that the population of surface fluorophores is either completely monomeric (m), dimeric (d), or trimeric (t). Results suggest the PCH method is capable of resolving the clustering states of fluorophores from the experimental photon counts, in accordance with previously reported experiments, based on the value of χ^2 [38]. Furthermore, the best fit with the best local χ^2 value is the 2-species fit with majority mEA1.

2.3.3 EphA2 activation by membrane associated EA1

After careful characterization of the membrane associated EA1 surface, MDA-MB-231 cells, a highly invasive breast epithelial cancer cell line that overexpresses EphA2 [40], are cultured on this surface and its EphA2 activation is measured. EphA2 triggering by membrane-associated ephrin-A1 has been previously characterized through the phosphorylation and degradation of this receptor tyrosine kinase [15]. These properties can be measured in two different manners: *i*) fluorescence microscopy to image immunostained signaling molecules colocalizing with EphA2 such as phosphotyrosine and the metalloprotease ADAM10, and *ii*) Western blot analysis to determine degradation and phosphorylation of EphA2. In this case, both methods are employed to determine EphA2 activation by membrane associated EA1.

First, to examine whether EphA2-expressing cells are responsive to changes in ligand concentration, MDA-MB-231 cells are incubated on different EA1 surfaces with different surface densities. The EA1 surface density can be titrated by changing both the solution incubation concentration and the molar percent of Ni capturing lipids incorporated into the supported membrane (Fig. 2.7A). The resulting mEA1 surface densities are measured using QF microscopy as previously described [37]. After 10 minutes of incubation, the cells are fixed and permeabilized. Fluorescently labeled antibodies staining for EphA2 and phosphotyrosine are imaged using epifluorescence microscopy (Fig. 2.7B).

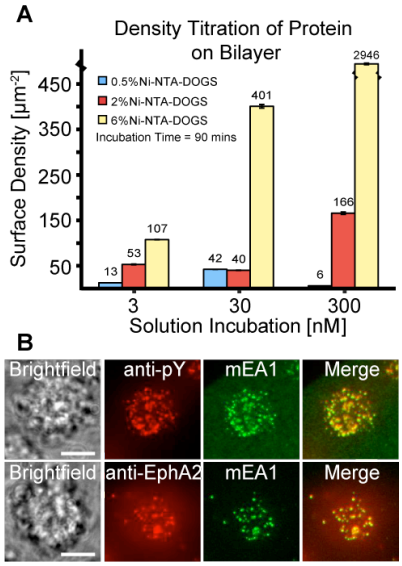

Figure 2.7. Surface density titration of mEA1 and immunofluorescence images of MDA-MB-231 cells. **A)** The surface density of mEA1 is titrated by varying the solution incubation concentration above the bilayer and the molar ratio of Nickel capturing lipids within the bilayer. The surface density measurements are performed using quantitative fluorescence microscopy. **B)** MDA-MB-231 cells are fixed and permeabilized after 15-minute incubations on these surfaces. Antibodies against phosphorylated tyrosine residues (pY) and EphA2 are used to detect phosphorylation at the regions of mEA1 cluster formation and to stain for the presence of EphA2, respectively. For high mEA1 surface densities (thousands of molecules/μm^2), phosphorylated proteins are recruited to the mEA1 microclusters. At low mEA1 surface densities (hundreds of molecules/μm^2), EphA2 is also recruited. These results suggest that over a range of surface densities, phosphorylated proteins and EphA2 co-localize with mEA1 on the single cell level. A similar result is observed for EphA2 at high mEA1 surface densities and pY at low mEA1 surface densities; recruitment of both molecules occurs over a range of mEA1 surface densities (results not shown). Scale bars are 10μm.

These representative images show the formation of EphA2 microclusters that colocalize with the microclusters of mEA1, imaged for the same cell. Similarly, phosphotyrosine immunofluorescence also colocalizes with mEA1 microclusters. The EphA2 receptor expressed on the membranes of MDA-MB-231 cells are interacting with membrane mEA1 proteins and there are high levels of phosphorylation, suggesting EphA2 activation. This colocalization is observed for mEA1 surface densities ranging from just a few molecules to hundreds molecules/μm^2. The membrane mEA1 fusion protein presented to MDA-MB-231 cells is capable of initiating receptor phosphorylation over a wide range of surface densities.

Next, the lateral reorganization and clustering of the mEA1 fusion protein is examined over the course of an hour. This incubation time is previously shown to be a useful observation time for the central transport of membrane EA1 by EphA2 expressing cells [15]. The EphA2 density on the surface of MDA-MB-231 is approximately several hundreds of molecules/μm^2; the surface density for mEA1 is fixed at a similar value for these experiments. Cells were fixed and permeabilized after incubations of 5, 10, 20, and 60 minutes for imaging (Fig. 2.8).

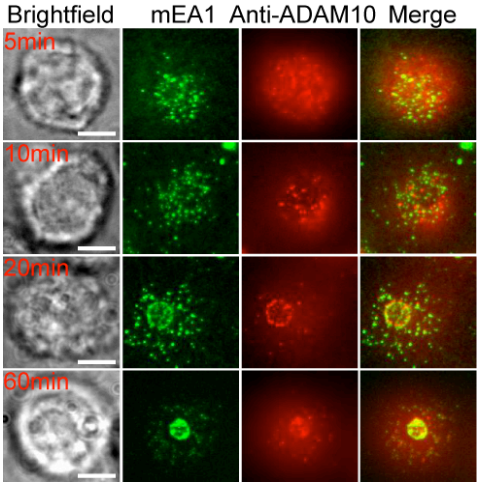

Figure 2.8. ADAM10 recruitment to mEA1 clusters in a spatiotemporal dependent manner. Time-dependent staining of MDA-MB-231 cells shows the formation of a central contact region at 20 and 60 minutes and subsequent recruitment of ADAM10. Cells are fixed and permeabilized after the indicated incubation time and imaged with epifluorescence microscopy. The surface density of mEA1 used in this experiment is approximately a few hundreds of molecules/μm^2. Anti-ADAM10 antibody clusters tighten at longer time points, colocalizing with mEA1 clusters, and therefore demonstrates that ADAM10 recruitment to the mEA1 clusters occur at later times when mEA1 has undergone radial transport. Scale bars are 10μm.

At early time points (5 and 10 minutes), Eph-ephrin clusters are generally micron-sized or smaller and are randomly distributed across the cell-SLB interface. Within 1 hr of cell engagement, these clusters coalesce into larger clusters that are transported to the center of the cell-SLB interface, resulting in a central contact zone several microns in diameter enriched in Eph-ephrin complexes. Temporal progression of ADAM10 recruitment to Eph-ephrin clusters is examined through staining cells with a fluorescently labeled anti-ADAM10 antibody. ADAM10 recruitment is a known step the EphA2 degradation pathway, and is thought to enzymatically cleave the ephrin ligand from the ligand-presenting surface [13]. At early time points (5 and 10 minutes), most of the ADAM10 is within the cell, well out of the focal plane of the objective, resulting in a blurred ADAM10 signal observed using epifluorescence microscopy. At later time points (20 and 60 minutes), we observe recruitment of ADAM10 to the EphA2-mEA1 clusters. A qualitative analysis of the fluorescence microscopy images suggest that mEA1 leads to EphA2 phosphorylation and degradation as mediated by ADAM10. Furthermore, these results suggest that ADAM10 recruitment to Eph-ephrin clusters is a dynamic process.

Lastly, to contextualize these findings within the framework of classical biochemical techniques, Western blotting is used to examine EphA2 phosphorylation and degradation across a wide range of mEA1 surface densities and preclustered states (Fig. 2.9 – 2.11).

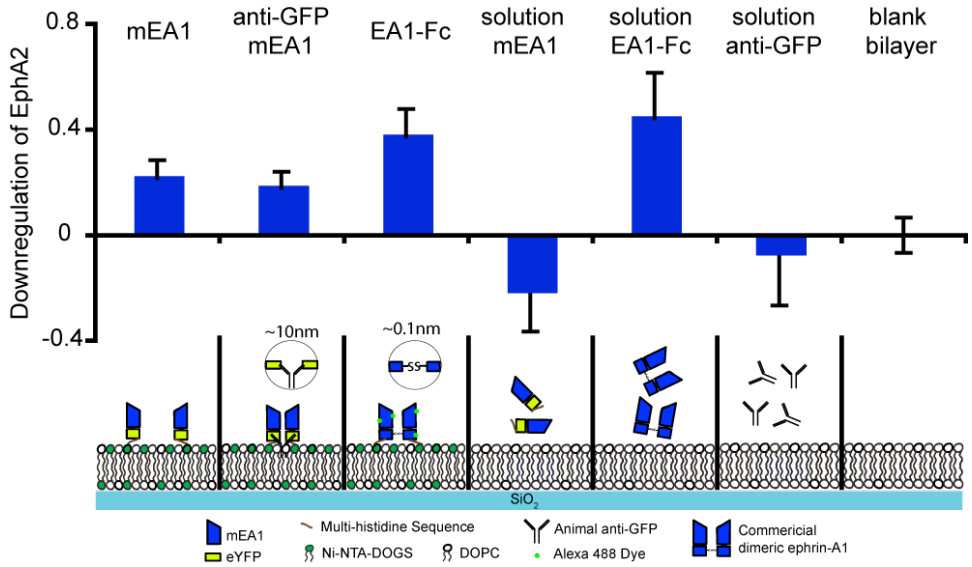

Figure 2.9. Western blots are analyzed from the lysate of MDA-MB-231 cells incubated on different surfaces and in different solutions. The blots are stained for the presence of EphA2. In this case, the degradation of EphA2 is represented by the intensity of an EphA2 band between 75 and 150 kDaltons. The lower the band intensity, the greater the receptor degradation. Intensity measurements of EphA2 bands are repeated for at least 4 unique Western blots and the results are averaged across the blots. Soluble mEA1, over a range of concentrations (results not shown), does not induce significant EphA2 degradation while mEA1 on a SLB leads to EphA2 degradation. Antibody crosslinked mEA1 on a SLB leads to EphA2 degradation, although to a lesser degree than preclustered EA1-Fc. At low surface densities of mEA1, Western blot analysis is unable to detect significant EphA2 activation (Fig. S7-S8).

MDA-MB-231 cells are incubated on surfaces displaying different surface densities and aggregation states of mEA1, including both membrane bound as well as in solution. After 2 hour incubations, the cells are lysed and the protein supernatant is analyzed. Exogenous dimerization is introduced using an anti-GFP mouse monoclonal IgG2a antibody to crosslink mEA1-eYFP-H10. A further degree of clustering is introduced through the addition of a goat anti-mouse IgG2a antibody. At low surface densities of EA1 (~100 molecules/μm^2) on the SLB, no significant EphA2 degradation or phosphorylation is observed regardless of the degree of EA1 crosslinking. Notably, this contrasts sharply with microscopy data, which indicates strong activation at similar densities. We speculate that Western analysis is not sufficiently sensitive to monitor signaling at these lower EA1 levels.

When the EA1 surface density is increased 10-fold (~1000 molecules/μm^2), EphA2 degradation and phosphorylation levels for mEA1 is measured at similar levels to those observed in response to soluble EA1-Fc, the synthetically crosslinked ephrin-A1 dimer. However, the membrane-bound antibody crosslinked mEA1, designed to mimic the EA1-Fc, is not as activating as the EA1-Fc presented on a supported membrane through a Ni-Histidine linkage. To explain this discrepancy, the length scales of the two different crosslinking strategies need to be examined. For the antibody crosslinked mEA1, the distance between two antigen binding sites of an antibody is approximately 10 nm [41], and this spacing might be unfavorable for EphA2 activation. On the other hand, the EA1-Fc dimer is linked by a disulfide bond, which is approximately 0.1 nm in length. This observation is consistent with the small length scales required for the recruitment of proteins in Eph signaling that has been previous reported [42].

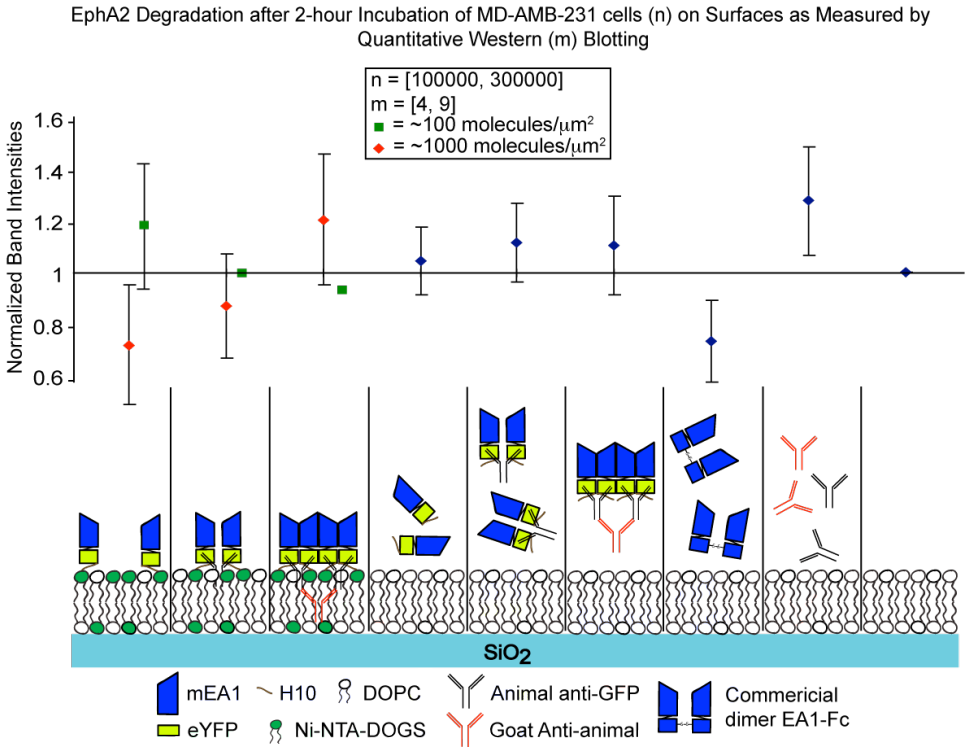

Figure 2.10. Western blot analysis of EphA2 degradation at low and high surface densities of mEA1 fusion protein. Several Western blots (m) are performed and are stained for EphA2. The intensity of the EphA2 band is measured between 75 and 150 kDaltons. This measurement is averaged across at least 4 independent Western blots. A lower number of the band intensity corresponds to higher EphA2 degradation.

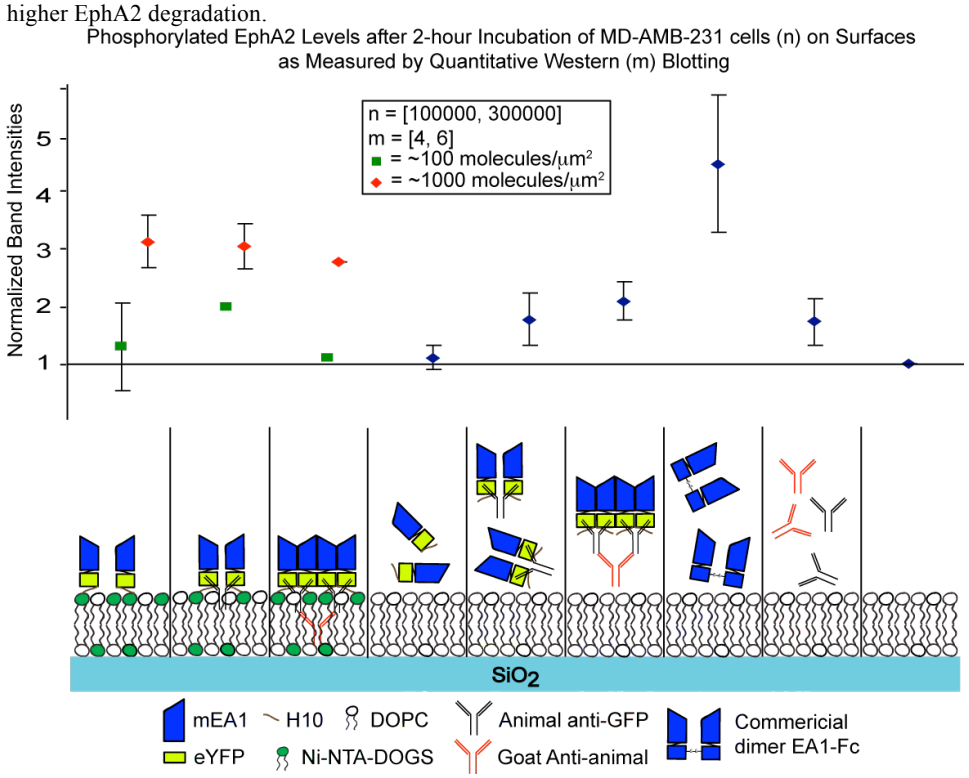

Figure 2.11. Western blot analysis of EphA2 phosphorylation at low and high surface densities of mEA1 fusion protein. The blots are stained for phosphotyrosine bands between 75 and 150kDaltons, where EphA2 is observed. A higher value for the band intensity represents more phosphorylated EphA2.

Similar to previous reports of the inactivity of soluble monomeric ephrin-A1 [26], we also observed inactivity of the mEA1-eYFP-H10 in solution for both EphA2 degradation and phosphorylation Western blot analyses. Although fluorescence microscopy measurements suggest that EphA2 can be activated by membrane EA1 over a range of surface densities, Western blot analysis is only capable of detecting EphA2 activation at high densities of membrane EA1.

To extend observations beyond the MDA-MB-231 cell line, the central transport of membrane mEA1 by EphA2 expressing cells is also observed for other breast cancer cell lines (Fig. 2.12). After an hour incubation on supported membranes with EA1 surface densities of ~100molecules/μm^2, a similar EA1-bound EphA2 transport leading to a central contact zone is observed. Immunofluorescence images of EphA2 show the receptor colocalizing with mEA1. The enhanced fluidity of the Ni-histidine anchoring strategy allows for a kinetically faster central transport as compared to the synthetically crosslinked ephrin-A1 dimer on supported membrane as demonstrated previously [15].

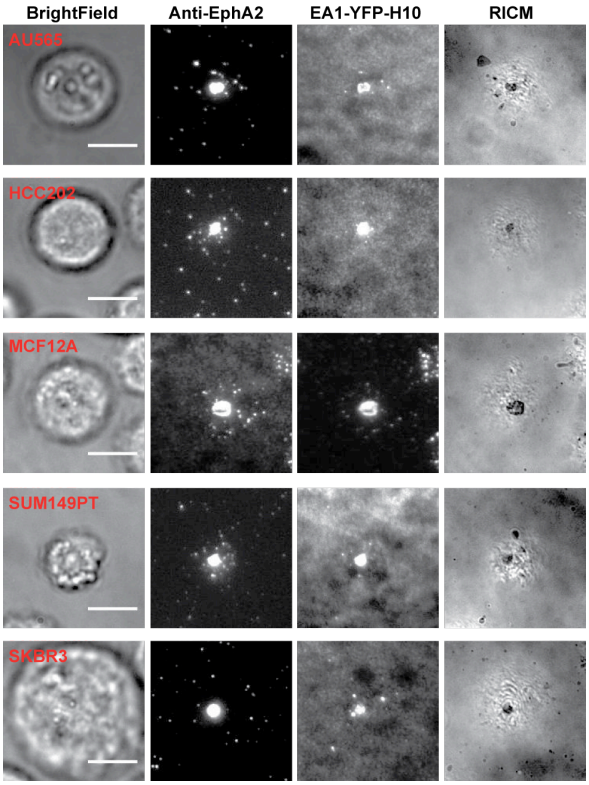

Figure 2.12. Central transport of membrane EA1-bound EphA2 is observed for other breast cancer cell lines. Cells are fixed after 1hour incubation on membrane EA1 surface and immunostained with anti-EphA2 antibody. Images are taken using TIRFM. Scale bars are 10μm.

2.3.4 EphA2 signal regulation in MDA-MB-231 cells has spatio-mechanical dependency

Sensitivity of the EphA2 system to spatio-mechanical perturbation is tested using the spatial mutation strategy. Patterns of metal grids, prefabricated onto the underlying substrate, restrict the lateral mobility of membrane mEA1 as well as ligand-engaged EphA2 receptors on the live cell. Immunofluorescence images of phalloidin labeled actin and ADAM10 detected with epifluorescence and total internal reflection fluorescence (TIRF) microscopies, respectively,

show the altered downstream signals as a consequence of EphA2 spatial mutation. When Eph-ephrin clusters are laterally constrained within corrals larger than 5 microns in pitch, the actin cytoskeleton is concentrated in an annulus, immediately peripheral to the Eph-ephrin central assembly (Fig. 2.13), which is indicative of cell contraction from the ephrin-presenting surface. When grids with narrower pitches are prepatterned onto the underlying substrate, the cytoskeleton displays a spreading morphology, suggesting mesenchymal cell behavior [43].

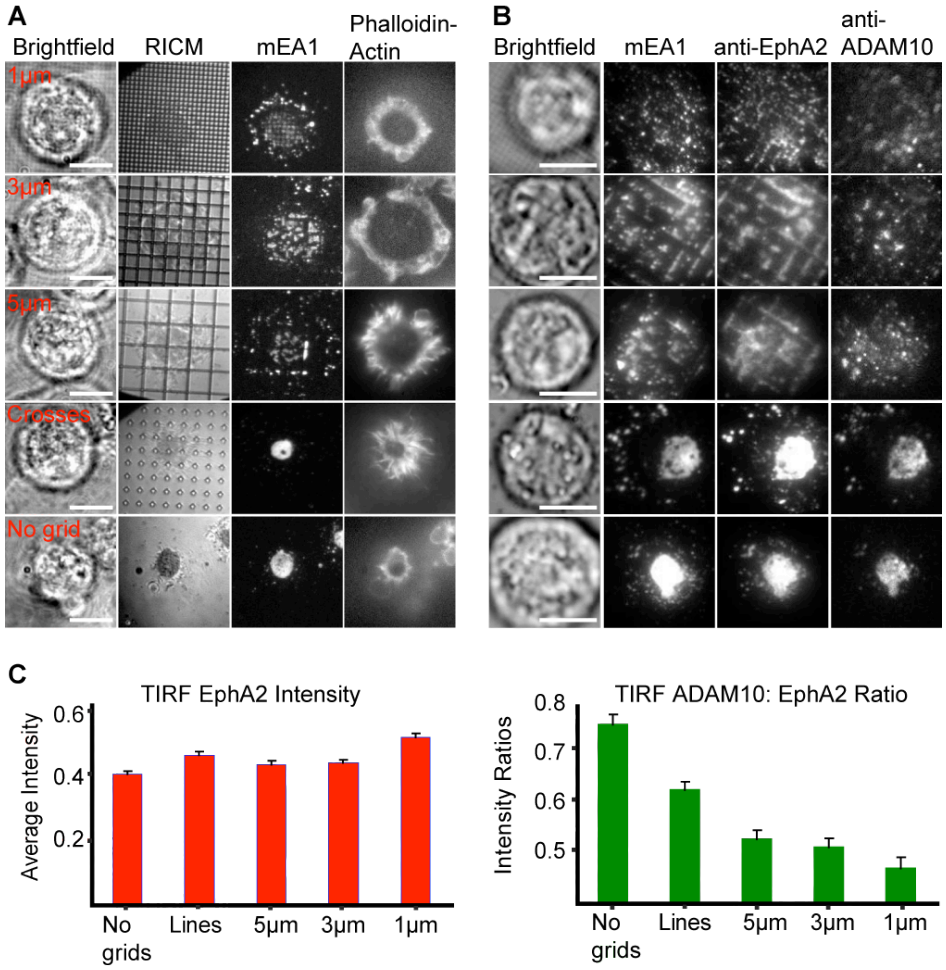

Figure 2.13. EphA2 pathway activated by mEA1 shows a spatio-mechanical regulatory component. **A)** Ligand-induced EphA2 clustering is restricted with chromium barriers. Epifluorescence images show cytoskeleton annulus formation when transport is unrestricted and cytoskeleton spreading morphology when transport is restricted. **B)** TIRF microscopy and **C)** subsequent quantitative colocalization analysis of EphA2 to ADAM10 reveals that ADAM10 recruitment occurs only when receptor transport is unhindered. An average of 200 cells were analyzed for each grid pitch. The surface density of mEA1 used for these experiments is approximately hundreds of molecules/μm^2. Scale bars are 10μm.

Using TIRF, which excites fluorophores within 70-100nm of the cell-SLB interface thereby eliminating a majority of the intracellular fluorescence signal [30], increasing ADAM10 recruitment is observed when Eph-ephrin transport is less hindered (Fig. 2.13B,C). The density of EphA2 on the membrane surface is equal across the different pitched corrals, suggesting that EphA2 recruitment to the cell membrane is unaffected by the Cr grids (Fig. 2.13C). These findings suggest that EphA2 signaling is sensitive to the lateral organization of membrane mEA1. Furthermore, this signaling pathway exhibits a dependency on the spatio-mechanical

organization of the EphA2 receptor.

2.4 CONCLUSIONS

Monomeric ephrin-A1 displayed on a supported membrane successfully triggers EphA2 in living cells. Importantly, this system enables observations of natural receptor ligand clustering and assembly processes, as driven by the EphA2 receptor expressing cell. We affirm some fundamental observations concerning influences of mechanical constraints of ephrin-A1 ligand movement on EphA2 signaling, which had been originally reported using only chemically crosslinked ephrin-A1 ligands. However, some differences in the kinetics of assembly are also noted between the two systems. Through the use of a monomeric fluorescent fusion protein of ephrin-A1, we are able to examine the initial steps of Eph-ephrin clustering and transport that have been shown to play vital roles in signal transduction and is functionally altered in cancerous cells.

2.5 Materials and Methods

2.5.1 Protein expression and purification

The soluble human monomeric ephrin-A1 (mEA1) sequence (Gift of Hans-Christian Åsheim, Oslo University, Norway) was cloned into the pN1-eYFP (Clontech Lab. Inc., Mountain View, CA) CMV expression vector with an A206K YFP mutation and was modified to contain a sequence of ten histidines directly after the eYFP portion according to published methods [24]. The expression vector was transfected into HEK 293T (Gift of Ann Fischer, UC Berkeley, CA) cells using Lipofectamine 2000 (Invitrogen Inc., Carlsbad, CA). The protein was purified with gravity flow column containing Nickel-Agarose beads (Qiagen Inc., Valencia, CA).

2.5.2 Ephrin-A1 modified SLB deposition

DOPC, 1,2-dioleoyl-*sn*-glycero-3-phosphocholine, and Ni-NTA DOGS, 1,2-dioleoyl-*sn*-glycero-3-[(N-(5-amino-1-carboxypentyl)iminodiacetic acid)succinyl] (Avanti Polar Lipids Inc., Alabaster, AL) vesicles were prepared according to published methods [44]. The hydrated lipid vesicles were sonicated using a tip sonicator (Sonics & Materials, Newtown, CT). Supported membranes were formed on glass coverslips from vesicles according to published methods [15]. The setup was then enclosed within an Attofluor cell chamber (Invitrogen Inc., Carlsbad, CA). To prevent non-specific binding of protein to the glass surface due to defects in the bilayer, the glass was blocked with 0.1% Bovine Serum Albumin (BSA, Sigma-Aldrich, St. Louis, MO). The mEA1-eYFP-H10 protein was added to the solution above the supported membrane at nM concentrations and allowed to chelate the Ni for more than 1.5 hours at room temperature. Excess protein was rinsed away and the solution was allowed to settle for 15 minutes to achieve the stable multivalent Ni-H10 association.

2.5.3 Membrane characterization

Epifluorescence Recovery After Photobleaching (FRAP). Images of a EA1-YFP-H10 modified SLB were taken on an Eclipse TE2000E (Nikon Instruments Inc., Melville, NY)

inverted microscope using a 100X 1.3 NA oil immersion objective (Nikon Instruments Inc., Melville, NY). The images were taken with a HQ CCD camera (Roper Scientific, Germany). The filter set used to set the excitation and emission wavelengths was a custom made YFP filter (Chroma Tech. Corp., Bellows Fall, VT). Metamorph (Photometrics, Tuscon, AZ) and ImageJ software were used to collect, analyze, and process the images.

Nickel Dissociation Curve. To ensure that mEA1 was anchored onto the SLB via a Ni-H10 linkage and that this linkage was stable within the time frame of the experiments, an mEA1-eYFP-H10 bilayer was rinsed with 1x TBS (Tris Buffer Saline) and imaged for every 30 minutes for 5 hours and then imaged again after 16 hours at room temperature. 100 mM EDTA was added at the end of 16 hours to compete with the H10 for chelating Ni. The same microscopy setup was used for this as for the FRAP measurements.

Quantitative Fluorescence Microscopy. The surface density of mEA1-eYFP-H10 on SLB was measured using a recently published technique [37]. Vesicles containing 0.01, 0.02, and 0.04 mole percent Bodipy FL DHPE (*N*-(4,4-difluoro-5,7-dimethyl-4-bora-3a,4a-diaza-*s*-indacene-3-propionyl)-1,2-dihexadecanoyl-*sn*-glycero-3-phosphoethanolamine, triethylammonium salt) (Invitrogen Inc., Carlsbad, CA) mixed with Ni DOGS-NTA and DOPC were prepared as reference lipid standards. The fluorescence intensities associated with each concentration was measured with the Eclipse TE2000E microscope. Following the bulk measurements, bilayers were created to contain a range of surface densities of the Bodipy lipids. The intensity at each surface density was measured using the same microscope and filter set as for the bulk calibration standards.

Fluorescence Correlation Spectroscopy (FCS) and Photon Counting Histogram (PCH). To determine the diffusion rate, a mEA1-eYFP-H10 bilayer was prepared as previously descibed. The Eclipse TE2000-E microscope was used. The illumination for the eYFP was provided using an 488nm Kr-Argon ion laser (Newport Corp., Irvine, CA). A custom-built confocal system equipped with hardware correlator (Correlator.com, Bridgewater, NJ) was used for FCS measurements. The confocal volume was calibrated by 100nM fluorescein in 1M NaOH solution. The autocorrelation functions were fitted to a simple, one-component, 2-dimensional model and the diffusion constant was back calculated from the calibrated confocal volume following published methods [45]. Data analysis software Igor (WaveMetrics Inc., Portland, OR) was used to analyze the autocorrelation function. Photon counting measurements were done using the same setup but the analysis followed standard methods [36,38]. The PCH data were analyzed using the Globals software package (Laboratory for Fluorescence Dynamics, Urbana-Champaign, IL).

2.5.4 Cell culture

Human breast cancer epithelial cell lines (ATCC, Manassas, VA) were cultured in serum-rich DMEM media supplemented with 10% fetal bovine serum, L-glutamine, and penicillin/streptomycin (all from Invitrogen Inc., Carlsbad, CA). In order to engage the cells with mEA1-SLBs, the cells were treated with trypsin-EDTA, centrifuged, counted, and added to each cell chamber (all from Invitrogen Inc., Carlsbad, CA).

2.5.5 Cell fixation and membrane permeabilization and immunostaining

For immunofluorescence experiments, cells were incubated on mEA1-eYFP-H10 SLB in a 37^{o}C,

5% CO_2 incubator. Cells were then rinsed with ice cold 1xPBS (Phosphate Buffer Saline) and fixed with 4% paraformaldehyde in 1xPBS. The membrane was permeabilized with 0.1% Triton-X-100 in 1xPBS. Cells were blocked with 1%BSA 1xPBS at 4°C overnight. The next day, cells were incubated with primary antibodies for 40 minutes in 1%BSA 1xPBS followed by secondary antibodies conjugated to Alexa dyes for 20 minutes. Phalloidin 350 (Invitrogen Inc., Carlsbad, CA) was used to stain for actin and was incubated with fixed and permeabilized cells for 20 minutes. The antibodies used were the following: 1° mouse monoclonal anti-ADAM10 A-3 (Santa Cruz Biotechnology, Inc., Santa Cruz, CA), 1° rabbit polyclonal anti-EphA2 (Millipore, Billerica, MA), 1° mouse monoclonal anti-phosphotyrosine, 4G10 (Millipore, Billerica, MA), 2° Goat anti-rabbit Alexa fluor 405 (Invitrogen Inc., Carlsbad, CA) and 2° Goat anti-mouse Alexa fluor 647 (Invitrogen Inc., Carlsbad, CA). The dilution factor for all antibodies was 1:100.

2.5.6 Quantitative Western blot analysis

Blotting. MDA-MB-231 cells were harvested from mEA1-eYFP-H10 SLB surfaces after incubation for 2 hours. First, each cell chamber containing 100,000 – 300,000 cells was incubated on ice and rinsed with a few mls of cold 1xPBS. Second, 100uL of NP-40 lysis buffer was added to the cell pellet. The cells on the glass surface were incubated in 50uL of NP-40 buffer and adhered cells were subsequently scraped off. The pelleted cells and the glass surface cells were combined and centrifuged. The supernatant containing lysed proteins were loaded onto SDS-PAGE protein gels. Western blots were performed for equally concentrated fractions of the cell lysates. Images were acquired using an infrared detection system (Licor Biosciences, Lincoln, NE).

Quantification. To quantify the levels of either EphA2 degradation or phosphorylation, ImageJ software was used to process the Western blots images. The intensity of the band corresponding to the correct weight (between 75KDa and 150 KDa) in each lane on the blot was selected and measured. The background was subtracted from this intensity value. The resulting value was normalized to the loading condition, which was the intensity of the actin band at 50kDa. This value was then normalized to the modified intensity for the negative control which is a cell chamber consisting of 300,000 cells on a blank 100% DOPC bilayer in each case. The antibodies used were the following: 1° mouse monoclonal anti-EphA2 D-7 (Millipore, Billerica, MA) at 1:250 dilution, 2° Goat anti-mouse Infrared 680nm (Invitrogen Inc., Carlsbad, CA) at 1:10,000 dilution, 1° Goat anti-actin I-19 (Santa Cruz Biotechnology, Inc., Santa Cruz, CA) at 1:2000 dilution, 2° Donkey anti-goat 680nm (Invitrogen) at 1:10,000 dilution, and 1° mouse monoclonal anti-phosphotyrosine 4G10 (Invitrogen) at 1:2000. The EA1- Fc (R&D Systems, Inc., Minneapolis, MN) was labeled with Alexa dyes according to published methods [15].

Antibody Crosslinking of mEA1-eYFP-H10. To crosslink the mEA1 fusion protein, the protein was incubated with 1° anti-GFP rabbit monoclonal antibody (Cell Signaling Tech., Danvers, MA) at 1:200 for 20 minutes to achieve dimers. For tetramers, first the primary and secondary antibodies were incubated together for 20 minutes using the previously described anti-GFP and a goat anti-rabbit in 1:200 dilution. This solution was then incubated with the protein for 20 minutes.

2.5.7 Metal patterning by electron-beam lithography

Chromium patterns were fabricated on 25mm diameter #1.5 round glass coverslips as previously

published [15]. To summarize, coverslips were piranha cleaned, then spin-coated at 1000rpm with ZEP 520A EB-resist (Zeon Chemicals, Japan) and conductive polymer (Mitsubishi Rayon, Carlsbad, CA). Resist was exposed via E-beam lithography (Crestec, Torrence, CA) at 100-150 μC/cm^2. Square grid patterns were fabricated to be 10nm thick and 100nm wide. The patterns have spacings of 1, 3, 5 and 20μm and crosses with spacing 3μm. Conductive polymer was rinsed with water and developed via sonication using isoamyl acetate. Cr was deposited by E-beam evaporation and resist mask was removed by sonication in methylene chloride.

2.5.8 Optical microscopy

Quantitative TIRF. TIRF microscopy was performed with a custom-built laser source as previously published [46]. To prevent overlapping emission signals, 3-color TIRF was achieved with 3 different lasers: 405nm (Coherent Inc., Santa Clara, CA), 488nm (Coherent Inc.), and 643nm (Crystalaser, Reno, NV). A T_i Eclipse microscope was used with an inverted TIRF 100X/1.49 NA oil objective (Nikon, Burlingame, CA). Images were acquired with an EM-CCD (Andor Inc., South Windsor, CT) using Metamorph software. To account for differences in the brightness of Alexa dyes and fluorescent proteins, calibration bilayers without cells containing the Alexa fluor 405, 647 and mEA1-eYFP-H10 were measured. The Alexa dyes were anchored to the bilayer through a biotin-streptavidin-biotin linkage according to published methods [15]. The ratio of differences in intensity was factored into the ratio and colocalization calculations below.
Colocalization Analysis. Methods used are similar to published protocols [15,47]. In summary, areas occupied by cells were chosen using cells in brightfield. These same areas were designated as regions of interest in ImageJ and cropped for further analysis. To determine the ratio of ADAM10/EphA2 fluorescence intensity, the net intensity in the ADAM10 (405nm excitation) channel was divided by the net intensity in the EphA2 (647nm excitation) channel, after factoring in the differences in the brightness of the dyes from the calibration bilayers.

2.5.9 Derivation

General autocorrelation function describing multiple diffusing components (N_i) with varied brightness (Q_i):

$$G(\tau) = \frac{\sum_i Q_i^2 N_i g_i}{\left(\sum_i Q_i N_i\right)^2} \qquad \text{(D1)}$$

For two-component system, this equation becomes:

$$G(\tau) = \frac{N_1 g_1 + Q^2 N_2 g_2}{(N_1 + Q_2 N_2)^2}$$

Furthermore, if we set:
$N_1 = F/N$
$QN_2 = (1-F)N$

We derive:

$$G(0) = \frac{Q + F(1 - Q)}{N} \quad \text{(D2)}$$

F: fraction of monomer
Q: average aggregation number
N: Number of monomer

Derivation of function relating fraction of monomer (F) to average aggregation number (Q) based on the autocorrelation function (Eq. D1) generated in FCS from the fluorescence fluctuations of freely diffusing fluorophores through a confocal spot [48]. Eq. D2 allows for the prediction of F for a given Q value. The size of the confocal spot is measured using fluorescein which has a consistent diffusion coefficient in solution.

Chapter 3

EphA2 Clustering in Invasive Cancer Cells Revealed by Single Molecules of Ephrin-A1 Presented on Nanoparticles

"Piled Higher and Deeper" by Jorge Cham, www.phdcomics.com

3.1 ABSTRACT

The EphA2 receptor tyrosine kinase, along with its biologically monomeric ligand ephrin-A1 (EA1), is implicated in highly invasive cancers. EphA2 overexpression is known to be a precursory signal to tumor maligancy in cancer cell lines and primary tumors. Although structural and biochemical studies reveal that overexpressed EphA2 receptors can cluster in a ligand – independent manner to form higher order assemblies, the mechanism of this process is not well understood. In this study, we create an experimental platform that displays immobile and fluid EA1 tethered to nanoparticles and supported lipid bilayers, respectively, to reveal EphA2 cluster formation in individual cells across ten different breast cancer cell lines. We find that the clustering phenotype of EphA2 of each cell line is strongly correlated to the invasiveness of the cell line. These results suggest EphA2 clustering is an elucidating property of invasive cancer cells, possibly enhancing their navigation through the basement membrane prior to metastasis.

3.2 INTRODUCTION

Eph receptors are RTKs that interact with its ephrin ligands in juxtacrine signaling and are responsible for the positioning, adhesion and migration of cells during early development.[49] Due to their role in normal cell behavior, this family of receptors and ligands are hijacked as main players in cancer cell invasion, metastasis, and angiogenesis.[50] In particular EphA2, which binds its biologically monomeric ephrin-A1 ligand on an apposed cell membrane, is overexpressed in 40% of breast cancers. Since EphA2 overexpression is highly correlated to invasive and metastatic tumors, much effort have been directed at developing therapeutics to target EphA2 expressing tumors by eliminating the EphA2 through antibody stimulation or targeting the cell to destruction by the native immune system.[51] Despite of the advantage of being target-specific, these methods do not target the mechanism by which invasion and metastasis occur. Recently, it is shown that the EphA2 receptor is sensitive to the mechanical perturbations of the external microenvironment and that downstream signals initiated by EphA2 are sensitive to the spatial organization of the receptor.[52] In addition, the *in vitro* invasion potentials of a panel of breast cancer cell lines are found to correlate with their ability to cluster ligand-bound EphA2 on supported lipid bilayers (SLB). Based on these reports, we hypothesize that EphA2 clustering phenotype is a malignant property of invasive cancer cells that can be exploited to distinguish invasive and metastatic cells from other cells within the same tumor.

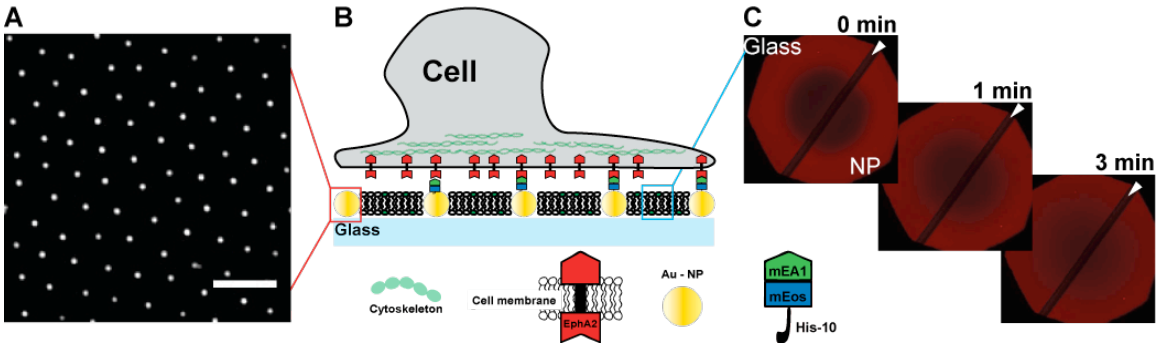

Figure 3.1. Schematic of the immobile EA1 – live cell SLB platform. **A)** Using scanning electron microscopy (SEM), we can image the hexagonal array of Au nanoparticles (NP) that are formed on the glass coverslip. **B)** Cancer cells expressing EphA2 incubated on the NP-glass surface can interact with single molecules of EA1 functionalized on individual Au NP. **C)** Fluid bilayers will form around the NP on the glass surface. Fluorescence recovery after photobleaching (FRAP) shows recovery of texas red lipids across the bare glass and NP-glass interface with similar diffusion rates. Scale bar is 200nm.

In order to observe EphA2 clustering in cancer cells, we created a novel platform of live cells cultured on a bilayer – Au-nanoparticle(Au-NP) interface by combining supported membrane technology with bottom-up nanotechnology (Fig. 3.1). In the previous chapter, it has been shown that chemically identical EphA2 expressing cancer cells can be cultured on and activated by a SLB anchored with homogeneously distributed, monomeric ephrin-A1 ligands.[53] Furthermore, functional proteins can be selectively and stably anchored to Au-NP within a SLB with proper orientation.[54] To achieve the bilayer – Au-NP interface, first, half of the surface of a round glass coverslip is patterned with an array of hexagonally ordered, highly monodisperse gold nanoparticles by dip-coating using block copolymer nanolithography.[55] In these experiments, the particle spacing is 100nm and the particle size is 7nm to match the thickness of the lipid bilayer (Fig. 3.1A). Second, a supported membrane is formed on this nanoparticle studded glass surface through the spontaneous fusion of phospholipid vesicles. Ephrin-A1 fluorescent fusion proteins that are genetically modified with C' terminal His10 tails are anchored on the nanoparticles and the phospholipids through a Nickel NTA-linker. The lipid composition of the supported membrane can be adjusted to contain NTA lipids that will capture ephrin-A1. Ligands tethered to the phospholipids remain fluid due to 2-dimensional diffusion along the surface while the same ligands anchored to the nanoparticles are immobile. Bilayer formation in the presence of gold nanoparticles has been previously characterized and shown to behave identically as the bilayer formed on the bare glass (Fig 3.1C).[54] Since the glass substrate is semi-patterned with Au-NP and ligand anchoring to either NP or phospholipid can be orthogonally controlled, this platform yields several unique configurations for live cell studies (Fig. 3.2A): i, fluid EA1 that is only anchored on the phospholipids (without immobile EA1 since Au-NP are not functionalized); ii, immobile EA1 that is only tethered to Au-NP (without fluid EA1 since phospholipids are not functionalized); and iii, a hybrid configuration with both fluid and immobile EA1 (both Au-NP and phospholipids are functionalized).

3.3 RESULTS AND DISCUSSION

3.3.1 MDA-MB-231 cells are sensitive to the presence of immobile mEA1

In the first experiment, MDA-MB-231 cells, a highly invasive breast cancer epithelial cell line, were cultured on a Au-NP glass surface displaying fluid EA1 that is only anchored on the phospholipids. After an hour incubation followed by fixation and membrane permeabilization, the cells were imaged using reflection interference contrast microscopy (RICM) which reveals regions of tightest adhesion between the cell and the SLB. In both the presence and absence of bare Au-NP, the MDA-MB-231 cells form tight central adhesion domains with the fluid EA1 (Fig. 3.2B). Similar to previous reports, immunofluoresence images of antibody labeled EphA2 receptor show its recruitment to these central adhesion domains where ephrin-A1 is highly concentrated. This recruitment is indicative of EphA2 activation in the MDA-MB-231 cells.[53] To investigate if fluid-only and immobile-only ligand presentations will lead to different signaling outcomes in terms of EphA2 recruitment, MDA-MB-231 were cultured on a glass substrate with only immobile EA1 and immunostained for EphA2. In this case, the RICM images taken of these

cells show adhesion areas that reflect cell spreading and filopodia protrusion formations (Fig. 3.2C).[40] Since the Au-NP is only patterned on half of the glass surface, the cells line up perfectly along the interface between the EA1-free bilayer side and the nanoparticle side (Fig. 3.3C), indicating that they will not interact with a EA1-free bilayer.

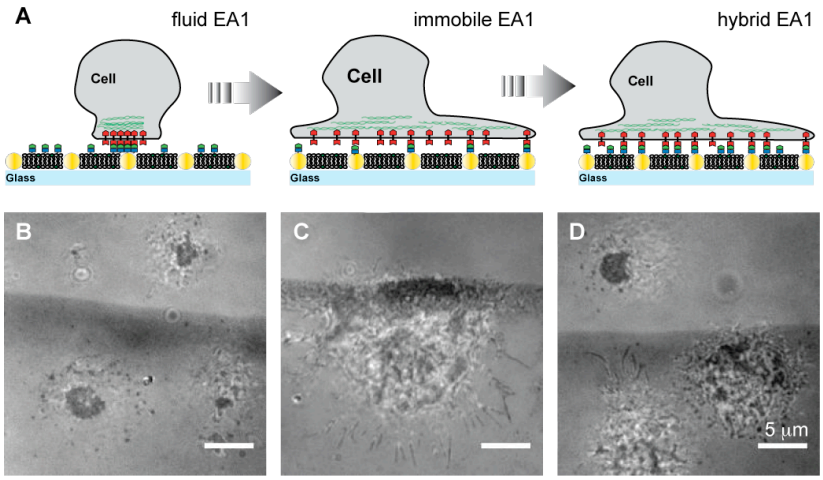

Figure 3.2. Three unique scenarios of EA1 presentation created from the NP-glass surface. **A)** Fluid EA1 refers to EA1 anchored to the lipid bilayer only; the NP are not functionalized with EA1. Immobile EA1 refers to a glass surface displaying only Au-bound EA1. The lipid bilayers around the NP do not contain capturing lipids that can anchor the proteins. In the last case, hybrid EA1 refers to both fluid and immobile EA1 states presented on the same surface. **B)** MDA-MB-231 cells cultured on the bare glass and NP-glass sides behave identically in terms their central transport of EA1-bound EphA2. The reflection interference contrast microscopy (RICM) image shows the region of tightest adhesion between the cell and the bilayer, revealing the central transport of EA1 on both sides. **C)** RICM image of MDA-MB-231 cells on the immobile EA1 shows a spreading phenotype and tight adhesions over a large area. **D)** RICM of MDA-MB-231 cells on the hybrid surface shows a combination of the two behaviors. On the glass side, with only fluid EA1, the cells centrally transport the EA1, whereas on the NP-glass side with the hybrid EA1 presentation, the cells adopt a spreading phenotype.

Immunofluorescence images of actin and EphA2 reveal the formation of actin protrusions, colocalizing with the RICM filopodia protrusions, that are studded with clusters of EphA2 receptors (Fig. 3.4). Higher resolution cellular morphological images, taken with scanning electron microscopy, show cellular protrusions along the nanoparticle arrays, reaching out to individual ephrin-A1 coated nanoparticles (Fig. 3.3 C.1-C.3). These images suggest that MDA-MB-231 cells interact with immobile EA1 substrates in a ligand specific, cytoskeletal driven manner involving the recruitment of EphA2. To control for non-specific cellular adhesion to the Au nanoparticles, these cells were placed on a glass surface with a EA1-free bilayer and EA1-free Au nanoparticles (Fig. 3.3B). Furthermore, to control for possible non-specific interactions between the cells and the NTA-linker, these cells were also placed on a glass surface with Ni-NTA lipids within the bilayer and NTA functionalized Au nanoparticles. In all instances, the controls verify that the MDA-MB-231 cells will only interact with the glass in the presence of EA1 either on the Au-NP or on the phospholipids. In the absence of EA1, the cellular interactions with the glass are few and random.

Since MDA-MB-231 cells can interact with fluid or immobile EA1 in manners that can be distinguished by cellular morphology and EphA2 cluster formation, these cells were cultured on a glass surface displaying both types of EA1 simultaneously because we want to determine if a morphology or recruitment preference will dominate. Notably, on a substrate with a hybrid configuration, the cells display the same spreading morphology and EphA2 clustering phenotype

as cells cultured on an immobile EA1 only surface (Fig. 3.2D and 3.4). However, on the exact same surface, the cells on the glass side without nanoparticles centrally transports EphA2 receptors into a large domain. These results suggest that the differences in cellular morphology and molecular recruitment between cells cultured on an immobile EA1 surface or a fluid EA1 surface are due to the presence of the immobile EA1 population which can enforce cellular morphological changes and EphA2 cluster formation. Despite of the presence of fluid EA1, the MDA-MB-231 cells interact with immobile EA1 preferentially.

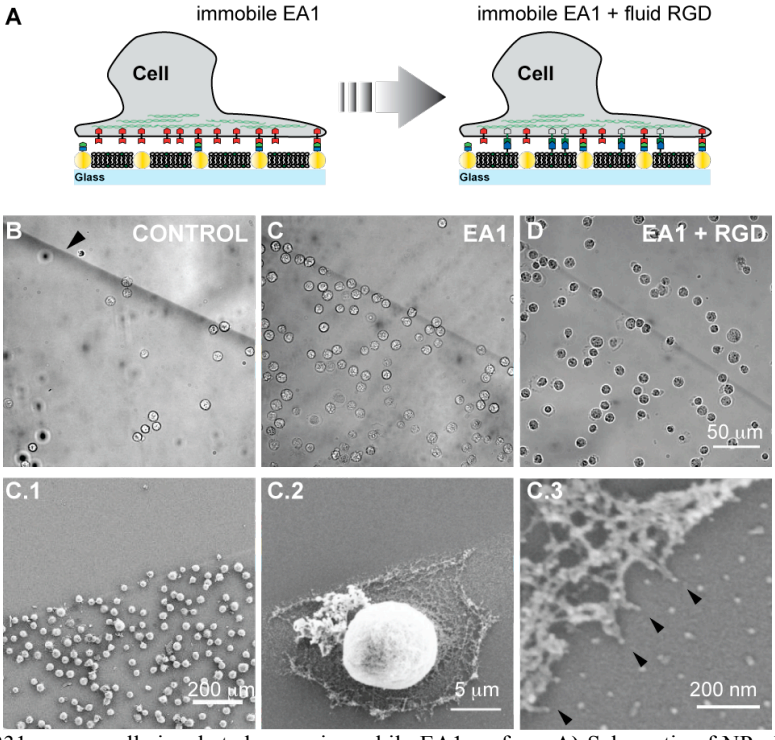

Figure 3.3. MDA-MB-231 cancer cells incubated on an immobile EA1 surface. **A)** Schematic of NP-glass with immobile EA1 on the NP. The lipid bilayer around the NP can be used to anchor proteins of interest. In this case, the schematic shows the integrin-interacting peptide, arginine-glycine-asparatic acid (RGD), anchored to the lipid bilayer as a control. Cells cultured on a blank NP-glass surface without EA1 do not bind to the NP particles as shown in the brightfield image in **B)**. Cells cultured on immobile EA1 surface preferentially bind to the NP glass side and no cells are observed on the bare glass side, as shown in **C)**. When RGD is anchored to the lipids, the cells can bind both the NP-glass as well as the bare glass sides. This control suggests that the bare glass side of a NP-glass coverslip will not prevent cells from interacting with signaling molecules anchored to this surface. Using Scanning Electron Microscopy (SEM), we also observed cytoskeleton protrusions spreading along the Au nanoparticles in the cells incubated on immobile EA1 surface, as shown in **C.1)-C.3)**.

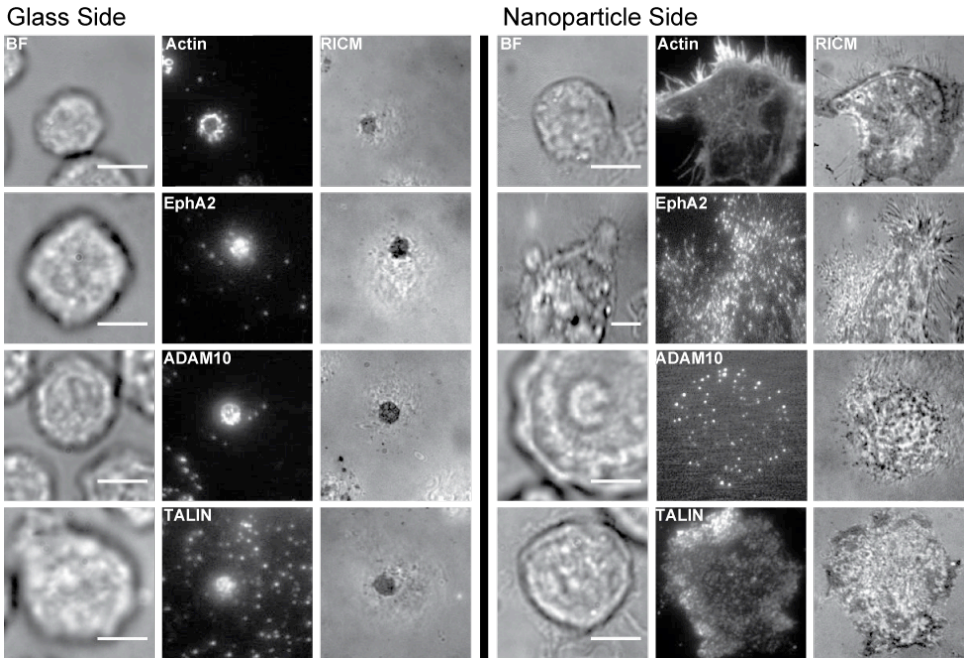

Figure 3.4. Immunostaining of different molecules in MDA-MB-231 cells cultured on the hybrid EA1 surface. Similar to before, MDA-MB-231 cells centrally transport EA1 on the glass side and recruit signaling molecules, ADAM10, Talin, and actin, which forms an annulus around the EA1. On the hybrid side, all of these signaling molecules show a spreading phenotype. Scale bars are 10 microns.

3.3.2 MCF10A cells are not sensitive to the presence of immobile mEA1

From these results we hypothesize that the strong affinity of MDA-MB-231 cells to immobile ephrin-A1 surface is a consequence of the invasive properties of this particular cell line. To test this, we selected an non-invasive epithelial cancer cell line, MCF10A, which has comparable EphA2 mRNA levels to the MDA-MB-231 cells.[40] After culturing these cells on the immobile ephrin-A1 surface with exactly the same incubation, fixation, and staining conditions as the MDA-MB-231 cells, the MCF10A cells did not attach (Fig. 3.5A – Immobile). This result suggests that MCF10A cells do not interact with a substrate displaying only immobile EA1. Therefore, the interaction between the EphA2 receptor, expressed on the MDA-MB-231 cells, and the immobile ephrin is not simply caused by the high mRNA levels in these cells. The ability of these cells to sense immobile EA1 may have a significant meaning in terms of how the EphA2 signaling pathway is deregulated; this ability is perhaps only possible when EphA2 receptors are clustered.

In the control sample with fluid ephrin-A1 only, MCF10A cells interact with the substrate and show central transport of the ligand-bound EphA2 receptor (Fig. 3.5A – Fluid). Culturing and comparing these two cell lines on the hybrid (immobile and fluid ephrin-A1) surface reveals a more intriguing difference: whereas the MDA-MB-231 cells shows two distinctly different phenotypes, no such difference is observed for MCF10A cells (Fig. 3.5A – Hybrid). While on the hybrid side, MCF10A cells can centrally transport ligand-bound EphA2, seemingly unhindered by the presence of immobile ephrin-A1, MDA-MB-231 displays clusters of EphA2 that are hindered by the presence of immobile ephrin-A1 (Fig. 3.5B–Hybrid). Since the immobile EA1 represents a nearly negligible percentage of the total EA1 surface density in the case of the hybrid system, cancer cells cultured on this substrate will therefore sense a majority of fluid

EA1. More importantly, the amount of fluid EA1 available to each cell is virtually unlimited due to its physical tether to the lipid bilayer, which renders it highly mobile and therefore easily transportable, while the surface density of immobile EA1 is practically limited by the amount of Au-NP underneath the cell. The large ratio of fluid EA1 to immobile EA1 in the hybrid configuration is the ideal probe for the sensitivity of the cell to the presence of the immobile EA1. This sensitivity is perhaps caused by the presence of EphA2 large clusters on the cell membrane and can be explained by the invasiveness of the particular cell line.

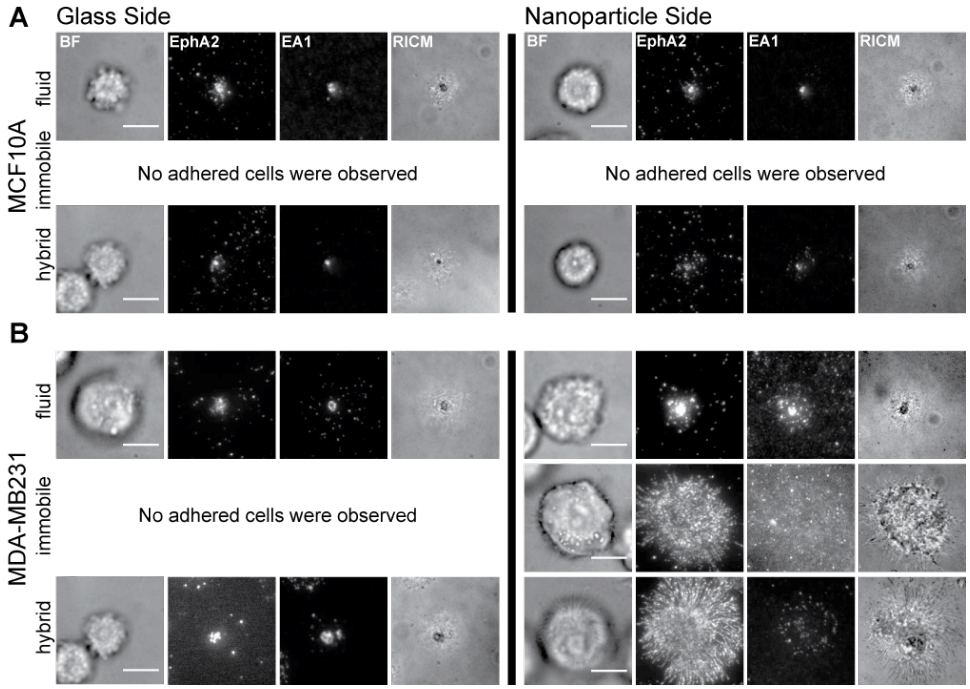

Figure 3.5 Comparing MDA-MB-231 cell line with MCF10A cell line on the three EA1 surfaces. **A)** When we cultured MCF10A cells on a fluid EA1 NP-glass surface, we find that EphA2 is centrally transported on both the bare glass side and the NP-glass side. When we culture the MCF10A cells on an immobile EA1 surface, we did not observe any adhered cells after fixation. Lastly, when we cultured the MCF10A cells on the hybrid EA1 surface, we find that the EphA2-EA1 complexes are centrally transported on both the glass as well as the NP sides. **B)** We cultured MDA-MB-231 cells on the fluid EA1 surface and find that EphA2 is centrally transported both sides, similar to before. When we cultured the MDA-MB-231 cells on an immobile EA1 surface, the cells bind only to the NP-glass side and spreads out. Using Total Internal Reflection Microscopy (TIRFM) we observe that cells form protrusions that contain EphA2 clusters along the mEA1 functionalized Au nanoparticles. In the last case, with MDA-MB-231 cells cultured on a hybrid surface, we find two different phenotypes on the same surface. On the bare glass side, cells still centrally transport EA1. However, on the hybrid side, EphA2 is transport is broken up into small clusters and MDA-MB-231 cells spread out with a phenotype similar to the behavior on the immobile EA1 surface. Scale bars are 10 microns.

3.3.3 Comparisons across 10 cancer cell lines reveal EphA2 cluster formation

To test this further, we extended our observations to eight more cancer cell lines, with varying degrees of invasion potentials and tumorigenicities, to determine if the affinity of EphA2 cluster binding to small fractions of immobile EA1 follows any measurable trend. Each cell line is individually cultured on a substrate with the hybrid configuration. The EphA2 clustering per cell line is measured by normalizing the EphA2 radial profiles of cells on the hybrid side to the EphA2 radial profiles of cells on the fluid side.[40] This normalization will eliminate data contamination due to cellular or experimental variability such as different EphA2 expression levels or variations in the staining protocol. The results for all cell lines are summarized in Figure 3.6: On the control side with fluid EA1 only, we find the ephrin-bound EphA2 receptor to

be centrally transported for all ten cell lines. Intriguingly, we find that across ten different cell lines, the normalized EphA2 radial transport is strongly correlated to the invasion potential of the individual cell line (Fig. 3.6A). For the five non-invasive cell lines, the EphA2 central transport remains unhindered in the presence of immobile EA1 on the hybrid surface (Fig. 3.6B). However, with increasing invasion potential, the EphA2 transport becomes interrupted and instead, small EphA2 clusters are spread across the interface between the cell and the hybrid surface.

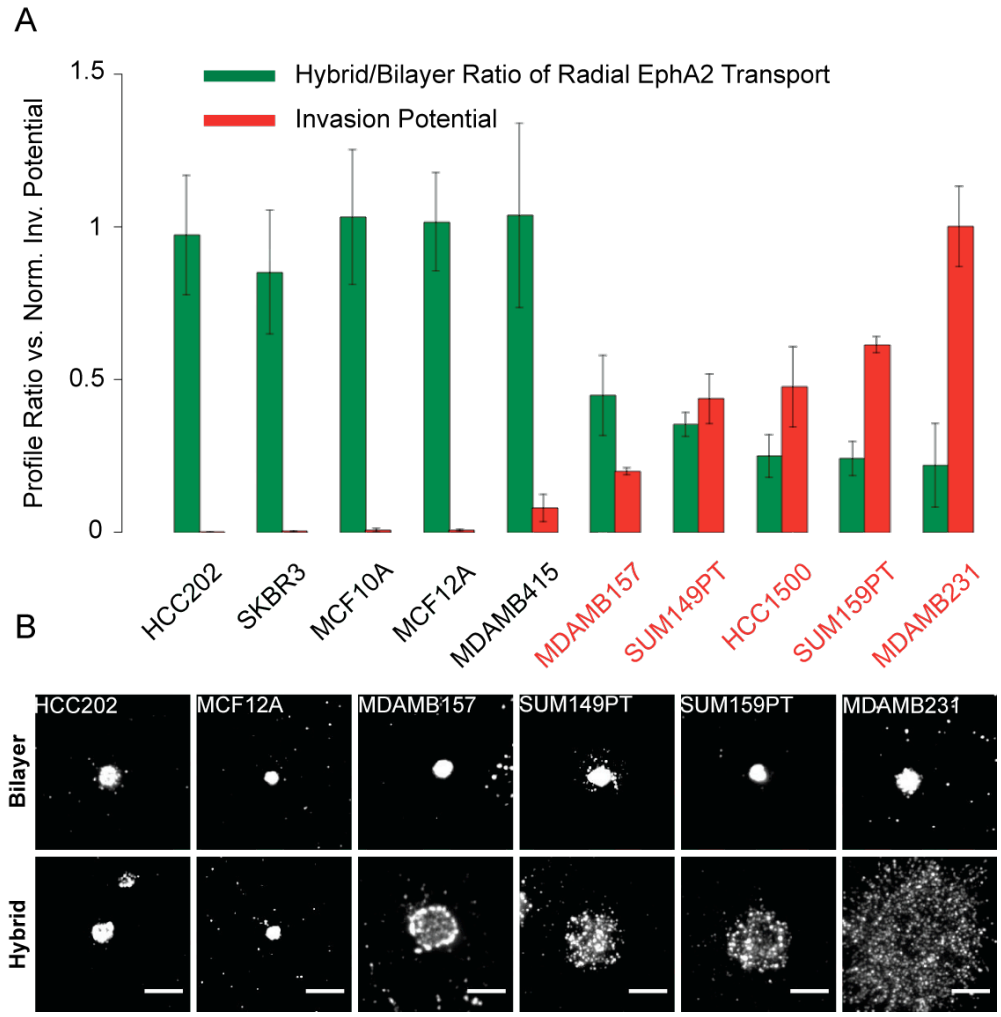

Figure 3.6. Breast cancer cell panel study. **A)** We studied the phenotypic change of a panel of breast cancer cell lines on our surface. We selected 5 non-invasive cell lines (black) and 4 invasive cell lines (red). Invasion potentials are obtained from a previous report using the modified Boyden chamber assay.[40] We find that when the invasion potential of the cell line increases, we observe a clustering tendency of EphA2 in cells on the hybrid side of the surface. For non-invasive cell lines, we observe the same centrally transported EphA2 phenotype for cells cultured on both sides. On the same glass surface, we can image cells cultured on a fluid mEA1 surface and cells cultured on a hybrid surface. The phenotypic changes we observe in cells cultured on the hybrid surface are normalized to the control cells within the same experiment. This would eliminate contributions from staining differences and cell to cell EphA2 expression variations. **B)** TIRFM immunofluorescence images of EphA2 of different cell lines cultured on the hybrid surface compared between the glass bilayer side and the hybrid side show the progressive formation of EphA2 clusters as the cell line increases in invasiveness. Scale bar are 10 microns.

The correlation of the EphA2 clustering phenotype with the corresponding invasion potential of the cancer cell lines supports and underscores past hypotheses about the role of increased concentration EphA2 clustering in invasive cancer cells.[17,56] We hypothesize that EphA2 clusters

are formed in invasive tumor cells to increase transport efficiency and quickly trigger cellular response. Therefore, these invasive cells are highly sensitive to the presence of a handful of immobile EA1 molecules within a sea of thousands of fluid EA1. In an invasive cell, the EphA2 clusters are hindered by single immobile molecules of EA1 because of a stronger binding due to avidity effects: in an EphA2 cluster of hundreds of molecules, when one EphA2 unbinds from EA1, another one can easily bind and therefore prevent the entire cluster from transport (Fig. 3.7A-C). In case of a non-invasive cell, EA1-bound EphA2 is centrally transported. Although individual EphA2 receptors can bind immobile EA1, it can easily unbind (Fig. 3.7D-F).

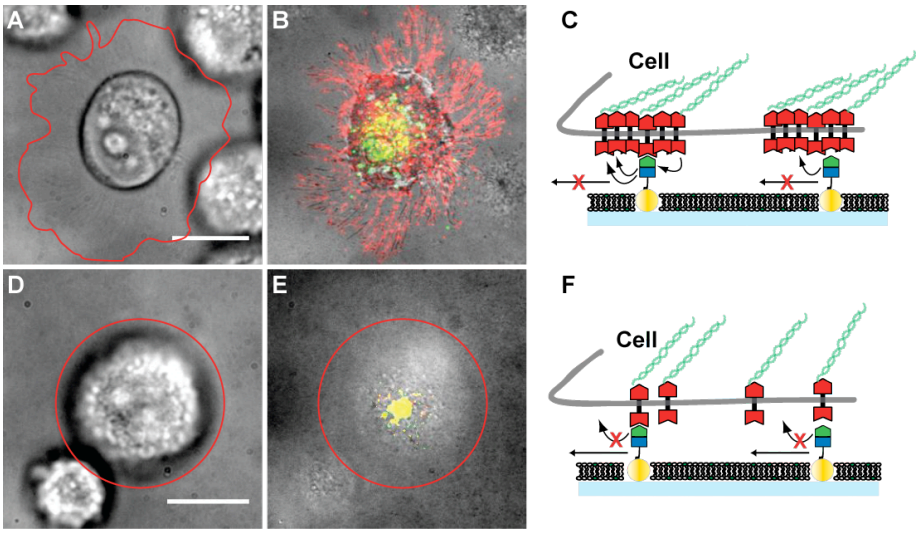

Figure 3.7. Model of EphA2 clustering. **A) – C)** We hypothesize that EphA2 cluster formation in invasive cell lines prevents the central transport of this cluster when several receptors are bound to immobile EA1 on Au-NP. When one EphA2 unbinds from EA1, another one close by can bind and therefore the clusters are not transported. Red color represents EphA2. Green represents EA1 and yellow represents a micron-scale colocalization between the two molecules. These colors are merged with an RICM image. **D)** We analyzed the cluster formation for a non-invasive cell line cultured on the hybrid surface and find that there is centrally transported where EphA2 colocalizes with EA1, **E)**. **F)** For the non-invasive cell lines, since EphA2 is not clustered, individual EphA2 can bind EA1 and unbind and become centrally transported when it binds to fluid EA1 in the lipid bilayer. Scale bars are 10 microns.

3.4 CONCLUSIONS

For the first time in single live breast cancer cells, EphA2 clustering has been observed with high resolution. To our knowledge, this has not been possible due to experimental limitations associated with reconstituting a juxtacrine signaling system in an *in vitro* setting and controlling the density and distribution of ligand presentation with nanometer resolution. Our results suggest that tumor cell invasion and metastasis are not only the result of EphA2 overexpression but also of the resulting receptor-receptor oligomerization process which sensitizes the cells to recognize a variety of EA1 ligand presentations, therefore paving compatible signal pathways for these deadly processes to proceed.

3.5 MATERIALS AND METHODS

3.5.1 Nanoparticle glass fabrication

Au-nanoparticle pattern on glass coverslips was prepared using Block Copolymer Micelle Nanolithography as previously published.[55] Diblock-Copolymer 1056 was dissolved in Toluene (Merck & Co. Inc., Whitehouse Station, NJ) at 4mg/ml; with constant stirring overnight. Stoichiometric amounts of HAuCl4*H2O was added to the polymer solution and stirred overnight with the following loading calculation:

$$m_{HAuCl4*H2O} = m_{PS\text{-}PVP} M_{HAuCl4*H2O} [VP]_n L / M_{PS\text{-}PVP};\ L \text{ (Loading)} \leq 1$$

The final loading parameter was 0.46. 25mm diameter #2 glass coverslips were cleaned for 30min in 2% Hellmanex in an Ultrasound bath and then for 20min in Piranha. Dip-coating of glass in the Au-polymer solution was achieved at 6x of the 4mg/ml solution. The dipping speed was set at 24mm/min. The subsequent Au coated glass was treated with plasma for 60 min and UV cleaned for 45 minutes.

3.5.2 Supported membrane formation

DOPC, 1,2-dioleoyl-*sn*-glycero-3-phosphocholine, and Ni-NTA DOGS, 1,2-dioleoyl-*sn*-glycero-3-[(N-(5-amino-1-carboxypentyl)iminodiacetic acid)succinyl] (Avanti Polar Lipids, Inc., Alabaster, AL) vesicles were prepared following previous methods.[19] To summarize, the desired lipids were mixed together and dissolved in chloroform in a piranha (3:1 of H_2SO_4: H_2O_2) – etched glass round bottom flask. The chloroform was evaporated using a rotary evaporator (Büchi, Flawil, Switzerland). This was further dried under N_2 gas and then hydrated with water. The hydrated lipid vesicles were sonicated using a tip sonicator (Cole-Parmer, Vernon Hills, IL). To form bilayers from the vesicles; first, the nanoparticle glass substrate was UV/Ozone treated for 20minutes; second, the substrate was allowed to fall unto a drop of lipid vesicle mixed with a spreading salt (1xTBS); third, the substrate was turned over under 1xTBS and enclosed within an Attofluor cell chamber (Invitrogen, Carlsbad, CA). Excess vesicles on top of the bilayer were rinsed away with 1x TBS.

3.5.3 Protein functionalization

Ephrin-A1 fusion protein with His10 tail, constructed as previously described[54], was functionalized on the Au nanoparticles through a dithiobisNTA (Dojindo Molecular Technologies, Inc., Sunnyvale, CA) linker.[53] The linker was reacted with the Au nanoparticles for 3 hours at room temperature. The protein was incubated in solution for 2 hours to functionalize both the supported membrane and the Au nanoparticles.

3.5.4 Cell culture

The human breast epithelial cancer cell line panel consisted of: HCC202, HCC1500, SKBR3, MCF10A, MCF12A, MDAMB231, MDAMB157, MDAMB231, SUM149PT, and SUM159PT. The HCC cells (ATCC, Manassas, VA) were cultured in RPMI supplemented with 10% fetal bovine serum (all were from Invitrogen Corp., Carlsbad, CA). The SKBR3 cells (ATCC) were cultured in McCoy's media supplemented with 10% fetal bovine serum (all were from Invitrogen Corp.). The MCF cells (ATCC) were cultured in DMEM/F12 supplemented with 20ng/mL

epidermal growth factor, 0.01 mg/ml bovine insulin (Sigma-Aldrich, St. Louis, MO), 500ng/ml hydrocortisone (Sigma-Aldrich), 5% horse serum, and 1% penicillin/streptomycin (unless otherwise indicated, all were from Invitrogen Corp.). The MDAMB cells (ATCC) were cultured in DMEM supplemented with 10% fetal bovine serum, 2mM L-glutamine, and 1% penicillin/streptomycin (all from Invitrogen Corp.). The SUM cells (generous gift from Joe W. Gray, Lawrence Berkeley National Lab, Berkeley, CA) were cultured in Hams/F12 media (Invitrogen Corp.) supplemented with 0.01mg/ml bovine insulin (Sigma-Aldrich), 500ng/ml hydrocortisone (Sigma-Aldrich), and 5% fetal bovine serum (Invitrogen Corp.). Prior to culturing cells on substrates, the cells were treated with 0.25% Trypsin-EDTA (Invitrogen Corp.) for several minutes, centrifuged, resuspended, counted, and then added to substrate.

3.5.5 Cell fixation and membrane permeabilization and immunostaining

Cells were incubated on substrates in 37^{o}C, 5% CO_2 incubator for 1hour. Cells were then rinsed with ice cold 1xPBS and fixed with 4% paraformaldehyde (Sigma-Aldrich) in 1xPBS. The membrane was permeabilized with 0.1% Triton-X (EMD Chemicals, Gibbstown, NJ) in 1xPBS. Cells were blocked with 1%BSA 1xPBS at 4^{o}C overnight. The next day, cells were incubated with primary antibodies for 40 minutes in 1%BSA 1xPBS followed by secondary antibodies conjugated to Alexa dyes for 20 minutes. Phalloidin 350 (Invitrogen Corp) was used to stain for actin and was incubated with fixed and permeabilized cells for 20 minutes. Between each incubation, the surface was rinsed with 1%BSA 1xPBS. The following antibodies were used: 1^{o} mouse monoclonal anti-ADAM10 A-3 (Santa Cruz Biotechnology, Inc., Santa Cruz, CA), 1^{o} rabbit polyclonal anti-EphA2 C-20 (Santa Cruz Biotechnology, Inc.), 1^{o} goat polyclonal anti-talin C-20 (Santa Cruz Biotechnology, Inc.), and 2^{o} Goat anti-animal Alexa fluor 647 (Invitrogen Corp.). The dilution factor for all antibodies was 1:100.

3.5.6 Microscopy

TIRF microscopy was performed with a custom-built laser source as previously described.[46] To prevent overlapping emission signals, 2-color TIRF was achieved with 2 different lasers: 488nm (Coherent Inc., Santa Clara, CA) and 643nm (Crystalaser, Reno, NV). A T_i Eclipse microscope was used with an inverted TIRF 100X/1.49 NA oil objective (Nikon, Burlingame, CA). Images were acquired with an EM-CCD camera (Andor Inc., South Windsor, CT) using Metamorph software. Scanning electron microscopy was performed at the Molecular Foundry, Berkeley, CA.

3.5.7 Data analysis

Areas occupied by cells were chosen using cells in brightfield. These same areas were designated as regions of interest in ImageJ and cropped for further analysis. The radial profile of EphA2 immunostained TIRFM images were processed using the Radial Profile plugin in ImageJ.

Chapter 4

Activation of EGFR Leads to Spatial Sorting with EphA2 Clusters

"Piled Higher and Deeper" by Jorge Cham, www.phdcomics.com

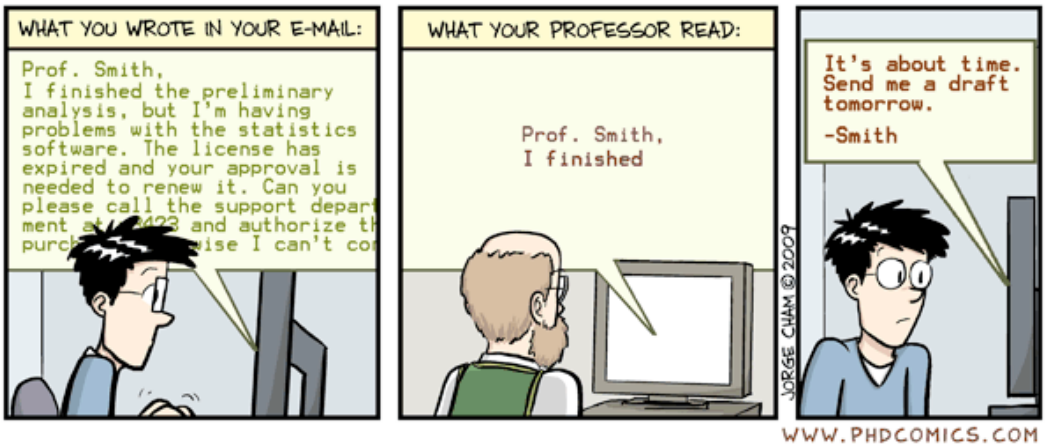

4.1 ABSTRACT

EphA2 and EGFR are members of different receptor tyrosine kinase families that are both overexpressed in many malignant cancers. EGF stimulated EGFR has been found to interact with EphA2 in biochemical assays however, the spatial organization of this behavior on the cell membrane is not well characterized. Anti-cancer drugs are being developed, through the creation of bispecific antibodies, to target both EGFR and EphA2 because of their relevant roles in cancer metastasis. In this chapter, we want to determine the signal crosstalk between EGFR and EphA2 on the cell membrane that is dependent on the spatial organization of the two receptors. We find that upon EGF stimulation, EGFR is spatially sorted to co-cluster with membrane-associated ephrin-A1 stimulated EphA2. Using DNA nanotechnology to create designer clusters, forcing EphA2 and EGFR to be transported together, we hope to understand how EGFR can be influenced by EphA2.

4.2 INTRODUCTION

The epidermal growth factor receptor (EGFR) is a receptor tyrosine kinase that is commonly involved in many malignant tumors as either an overexpressed or mutated protein [57]. Ligand stimulated EGFR, by soluble EGF, has been found to both interact with EphA2 and affect EphA2 expression [58]. Although EGFR activation can occur independent of ligand stimulation. The anti-cancer monoclonal antibody drug, Cetuximab, available on the market today to treat metastatic colorectal and head and neck cancers [59], specifically functions to interfere with the activity of EGFR. However, this drug has been found to be ineffective in a large subset of cancer patients and can lead to negative side effects. In light of these difficulties and the interactions between EGFR and EphA2, we aim to understand how these two receptors signal in breast cancer cell lines using the hybrid live cell – SLB platform and DNA nanotechnology. Cancer cells cultured on ephrin-A1 functionalized SLB and immunostained for EGFR show an exclusion effect between EphA2 and EGFR; the ligand-bound EphA2 is centrally transported to the cell-SLB adhesion area while EGFR remains on the periphery of this center. Interestingly, EGF stimulated EGFR forces this receptor to colocalize with EphA2. We hypothesize that EGFR and EphA2 signal pathways have significant crosstalk abilities that can be observed by their spatial organization patterns. This spatial exclusion effect can be explained in two different ways: upon stimulation of EGF, EGFR is driven into the center of the cell-SLB adhesion area independent of EphA2 or EGFR physically binds to EphA2 and is transported by EphA2 into the center. Using DNA nanotechnology, we can create designer clusters, forcing EGFR and EphA2 to travel together, to distinguish between these two scenarios. The result will be extremely fruitful since the intelligent design of bispecific antibodies is already underway for the treatment of EGFR and EphA2 related cancer metastasis.

4.3 RESULTS AND DISCUSSION

4.3.1 EGF stimulation directs EGFR co-localization with EphA2

MDA-MB-231 cells, which overexpressed both EGFR and EphA2[40], are stimulated with EGF for 2 days and then incubated on an ephrin-A1 supported membrane. After an hour of incubation, the cells are fixed and permeabilized and stained with anti-EGFR antibody. Using total internal reflection fluorescence microscopy (TIRFM), images taken of non-stimulated cells show EGFR as anti-colocalized with the ephrin-A1/EphA2 complex. This is apparent in the formation of an annulus-like ring structure (Fig. 4.1A). In these experiments, the location of the ephrin-A1, as a result of active transport through binding to EphA2, is taken as the location of EphA2. In stimulated cells, the EGFR is often colocalized with ephrin-A1/EphA2 complexes. Radial profile analysis performed on many cells show a similar trend. The ephrin-A1 transport to the center of the cell membrane – supported membrane contact region remains unaltered in both stimulated and non-stimulated cells (Fig. 4.1B). However, the EGFR radial profile shifts, when the cells are stimulated, toward the center.

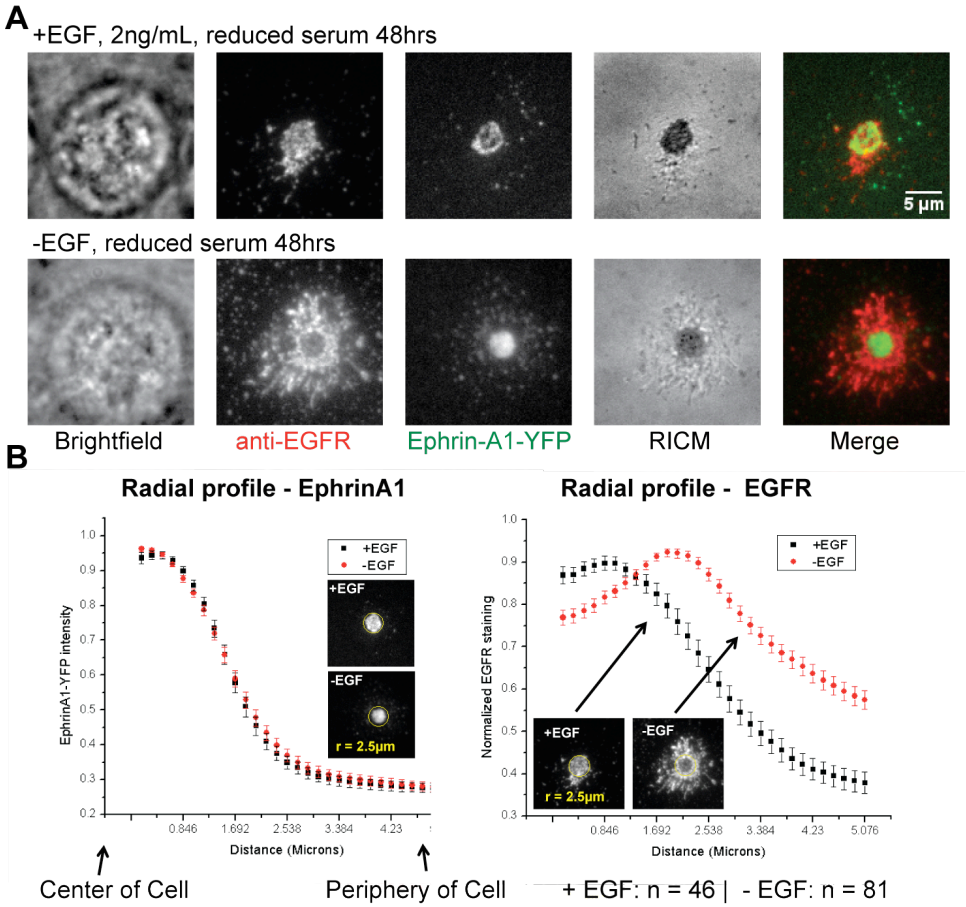

Figure 4.1. Long-term EGF stimulated EGFR is transported along with ephrin-A1 stimulated EphA2 to the center of the cell membrane – supported lipid bilayer interface. **A)** MDA-MB-231 cells are stimulated with EGF at 2ng/ml in solution for 48 hours in reduced serum media. The cells are subsequently stimulated by an ephrin-A1 supported membrane for 1 hour and fixed and permeabilized. Immunostaining with anti-EGFR antibody allows for observing the location of EGFR proteins on the cell membrane. In this case, the EGFR colocalizes with ephrin-A1 that has been transported by binding to the EphA2 in the cell. In the case of non-stimulated MDA-MB-231 cells grown in reduced serum, after ephrin-A1 stimulation, the majority of the EGFR resides on the periphery, forming a tight structure that seems to be distinctly excluded from the ephrin-A1 in the center. **B)** Radial

profile analysis performed on a total of 127 cells (n) show a similar trend as observed with immunofluorescence taken using TIRFM.

EGF stimulation of EGFR is sensitive both to the length of stimulation and concentration of EGF [60]. Since the 48 hour EGF stimulation might allow the cells to reach a steady state and give raise to bias, short term EGF stimulations are examined. MDA-MB-231 cells are first cultured in reduced serum conditions, to allow observations of EGF stimulation to be more dramatic, and then stimulated with EGF at the same time as being stimulated with ephrin-A1 on supported membranes. The cells are fixed and permeabilized after 16 and 64 minutes and stained for EGFR. The images are taken with TIRFM. At the 64 minute time point, we find that a similar exclusion effect is observed for this short-term EGF stimulation at the same concentration as the 48 hour, long-term EGF stimulation. The EGFR is excluded from the ephrin-A1 center in the case of non-stimulated cells and is colocalized with the ephrin-A1 in the case of stimulated cells (Fig. 4.2). At the 16 minute time point, the EGFR is distributed over the membrane surface without significant order in relations to the ephrin-A1 clusters.

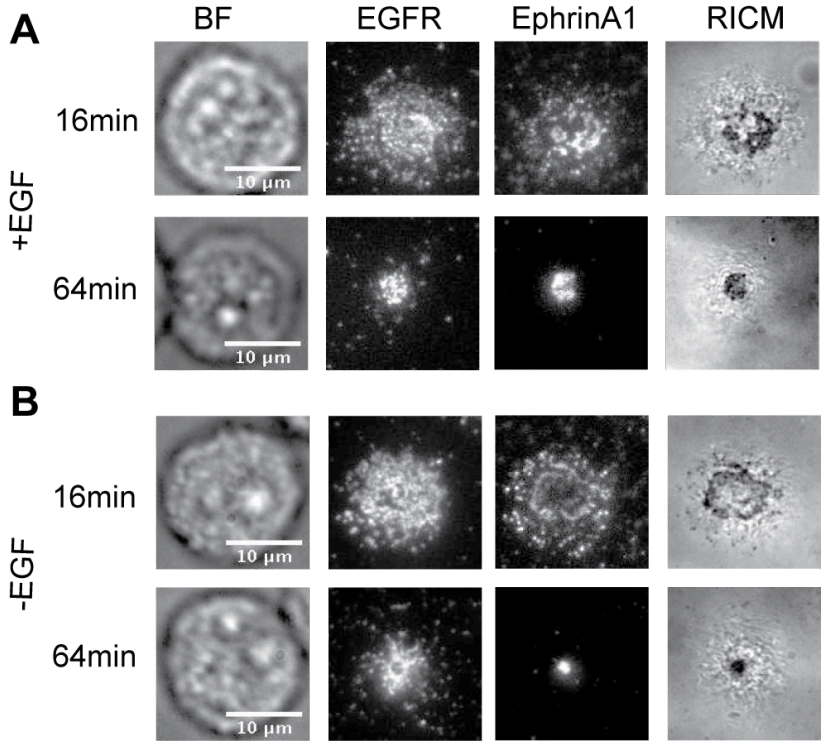

Figure 4.2. Short-term EGF stimulation of EGFR in MDA-MB-231 cells. **A)** After stimulation at either 16 or 64 minutes with soluble EGF and membrane-associated ephrin-A1, EGFR is concentrated in the center, where the ephrin-A1 is also found. **B)** For non-stimulated cells, at 16 minutes, the EGFR is randomly distributed across the cell membrane. At 64 minutes, the EGFR is also distributed across the cell membrane but largely depleted in the center, where the ephrin-A1 is found.

Since EphA2 signaling has been previously demonstrated to have a spatio-mechanical regulatory component, we wanted to examine the effects of spatial mutation on the signal crosstalk between EGFR and EphA2. Reduced serum MDA-MB-231 cells, cultured with and without EGF for 48 hours, are incubated on ephrin-A1 supported membranes in the presence of restricted ephrin-A1 diffusion. After an hour, we find that the presence of Chromium patterns do not by itself affect the spatial organization of EGFR and EphA2 bound ephrin-A1 (Fig. 4.3, 20µm). When the lateral diffusion of ephrin-A1 is restricted, the stimulated EGFR seems to colocalize with the

ephrin-A1 (Fig. 4.3, 5µm). In the case of the highest pitched Cr barriers and therefore the greatest restriction, the ephrin-A1 is scattered over the cell membrane and the EGFR is randomly distributed over the cell membrane, underlying the spreading morphology of these cells. We conclude from these results that activated EGFR is within clusters of ephrin-A1 stimulated EphA2. However, the signal significance of this co-transport needs to be examined. Since EGF stimulation may not lead to EGFR phosphorylation, which is a hallmark of RTK activation[4], we next look for the location of phosphorylated EGFR (pEGFR).

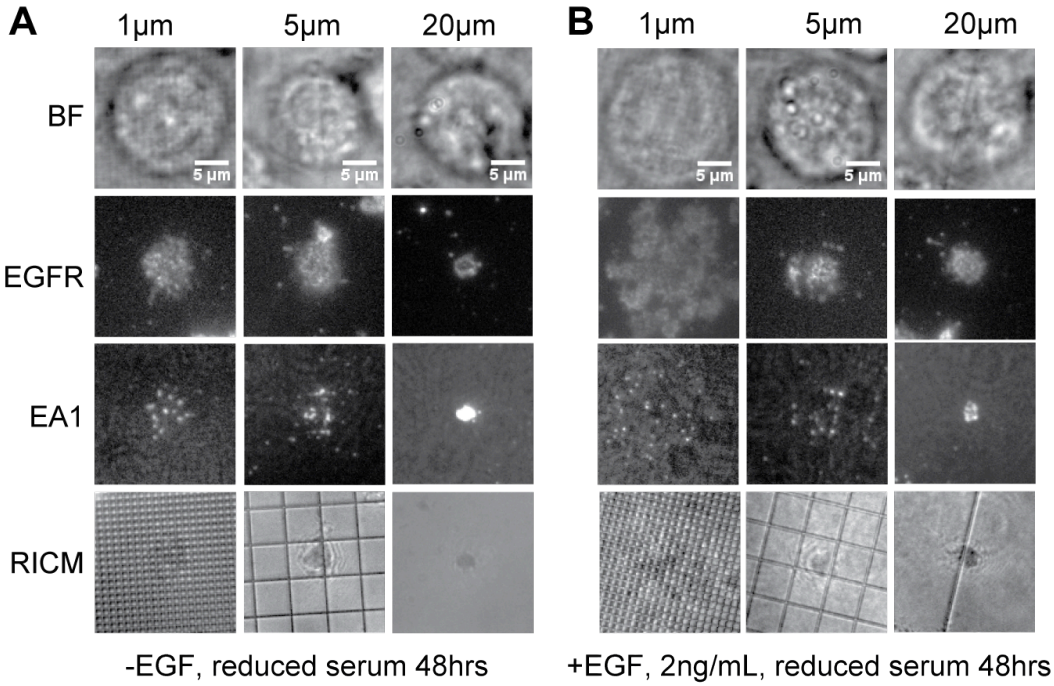

Figure 4.3. Spatial mutation of the ephrin-A1 supported membrane. **A)** Non-stimulated MDA-MB-231 cells are incubated on different pitched gridded surfaces and stained for EGFR. In the 1µm pitched case, the EGFR organization does not show any distinctive organization. For the 5µm and 20µm cases, the EGFR anticolocalizes with ephrin-A1. **B)** Stimulated MDA-MB-231 images show a similarly ambiguous organization in the 1µm pattern. For the 5µm and 20 µm patterns, the EGFR is colocalized with ephrin-A1 clusters.

4.3.2 Spatial sorting of activated EGFR

One method of detecting phosphorylated EGFR is to stain fixed and permeabilized cells with antibodies for pEGFR. In our case, reduced serum MDA-MB-231 cells are stimulated with EGF for 48 hours, incubated on an ephrin-A1 supported membrane, and fixed after 1 hour. We used a combination of pEGFR antibodies that would recognize different phosphorylation sites on the EGFR receptor. We find that regardless of EGF stimulation, the pEGFR is located in the center, colocalizing with ephrin-A1 (Fig. 4.4).

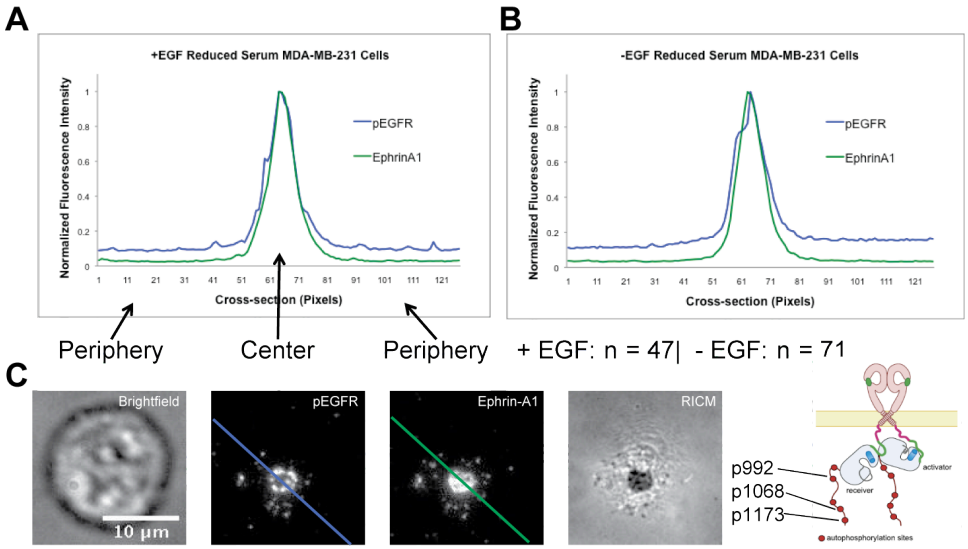

Figure 4.4. Staining for pEGFR in MDA-MD-231. **A)** Cross section analysis of stimulated cells show the highest fluorescence intensity in the center of the cell. This result is also seen for unstimulated cells in **B)**. The antibodies for the pEGFR are for three unique phosphorylation sites on the C-terminus of the protein [61]. **C)** Representative TIRFM images show pEGFR colocalizing with ephrin-A1.

This result is not surprising, since EGFR is constitutively active in the highly invasive MDA-MB-231 breast cancer cells. Therefore, this activity can make it difficult to distinguish between EGF stimulated phosphorylated EGFR and endogeneously phosphorylated EGFR. To overcome this, we examined another cell line, MCF12A. This cell line has comparable levels of EphA2 and EGFR as the MDA-MB-231 cell line but it requires EGF to grow and therefore, does not have constitutively active EGFR. Furthermore, these cells are non-invasive and non-tumorigenic[40]. Since antibody crosslinked EGFR is commonly used to stimulate this receptor [62], this effect was also examined in our system. MDA-MB-231 and MCF12A cells are cultured in reduced serum media for 24 hours prior to incubation on ephrin-A1 supported membrane and subjected to EGF stimulation for an hour. The cells are fixed and immunostained with anti-pEGFR-p1173. The results show that for regular EGFR, both stimulated MDA-MB-231 and MCF12A cells have a higher phosphorylated EGFR signal than the respectively non-stimulated control cells (Fig. 4.5). When EGFR is crosslinked, it is phosphorylated at the 1173 site regardless of EGF stimulation. These results are consistent with past observations of RTK crosslinking leading to activation.

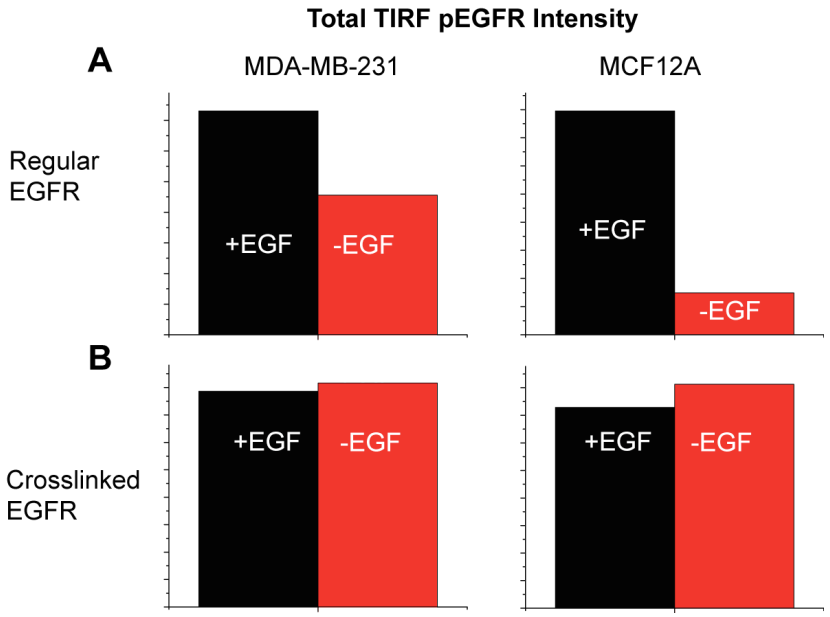

Figure 4.5. MDA-MB-231 and MCF12A cells are stimulated with EGF. **A)** For uncrosslinked EGFR, MDA-MB-231 and MCF12A cells show similar trends. When the EGFR is crosslinked with an antibody on the cell membrane, it becomes phosphorylated regardless of EGF stimulation in both cell lines.

Since EGFR phosphorylation after EGF stimulation occurs within minutes of adding EGF, shorter time points are examined. We hypothesize based on live cell movies that in stimulated cells, phosphorylated EGFR colocalizes with EphA2 bound ephrin-A1 clusters within 20 minutes of stimulation. To test this, MDA-MB-231 cells are fixed after 16 minutes and the pEGFR intensity is only measured within ephrin-A1 clusters (Fig. 4.6). To analyze the TIRFM images, a mask is created around the ephrin-A1 clusters and the pEGFR and EGFR intensities are measured within these regions. We find that pEGFR is concentrated in ephrin-A1 clusters when the cells are stimulated. Interestingly, there is less EGFR in these clusters for the stimulated cells as compared to the non-stimulated cells. These results can be explained by the endocytosis of activated EGFR which occurs within minutes of EGF stimulation.

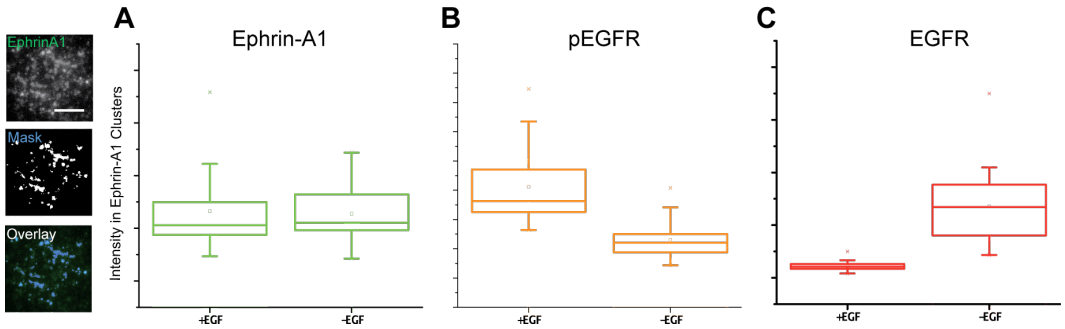

Figure 4.6. EGFR and pEGFR within ephrin-A1 clusters. MDA-MB-231 cells are stimulated with EGF for 48 hours at 2ng/ml and incubated on ephrin-A1 supported membranes for 16 minutes. Box and Whisker plots show **A)** Ephrin-A1 intensity to be the same in both stimulated and non-stimulated cells. **B)** Phosphorylated EGFR is higher in stimulated cells and lower in non-stimulated cells, within the ephrin-A1 clusters. **C)** EGFR shows an opposite trend in that when it is stimulated with EGF, there is less EGFR in the ephrin-A1 clusters. A total of 59 cells were analyzed.

4.4 FUTURE DIRECTIONS

EGFR is spatially sorted relative to EphA2, travelling with EphA2-bound ephrin-A1 clusters in an EGF dependent, phosphorylated manner. From these observations, we hypothesize that a disruption of EGFR and EphA2 spatial organization on the single molecular scale will change the outcome of EGFR phosphorylation. In other words, EGFR can be activated if it is forced to transport with ephrin-A1 stimulated EphA2. This hypothesis is based on our observations that within EphA2-bound ephrin-A1 clusters, EGFR is phosphorylated as a result of EGF stimulation. To test this, we plan to use DNA nanotechnology to make designer clusters of ephrin-A1 and anti-EGFR on the supported membrane (Fig. 4.7). MDA-MB-231 and MCF12A cells will be incubated on these surfaces and the intensity of phosphorylated EGFR will be measured within ephrin-A1 clusters.

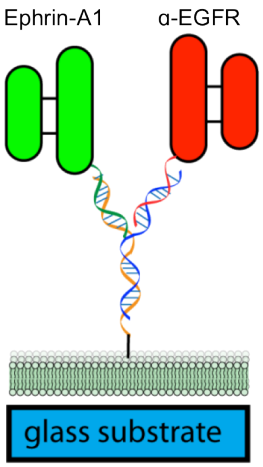

Figure 4.7. Designer cluster of ephrin-A1 and anti-EGFR on supported membrane.

The development of personalized medication is an emerging field in breast cancer diagnosis and treatment. The nascent stages of such a development requires having the strategy that can, for example, control many different signaling molecules within a pathway involved in cancer cells. This method of using DNA is fueled by the hope of one day having complete control of both the composition and concentration of proteins within a cluster of a designer shape that can induce a specific reaction in breast cancer cells and perhaps, cause the previously invasive cells to stay and adhere.

4.5 MATERIALS AND METHODS

4.5.1 Antibody labeling of EGFR

Fab fragments of EGFR Ab-11 (clone 199.12, LabVision, Fremont, CA) have been shown not to activate the receptor or interfere with ligand dependent activation of the receptor [63]. The antibody was first labeled using the Alexa Fluor 594 monoclonal antibody labeling kit (Invitrogen, Inc., Carlsbad, CA). The labeled antibody was digested with a Fab micropreparation kit (Thermo Fisher Scientific, Inc., Rockford, IL), which was used according to the manufacturer's directions. Briefly, the antibody was digested with resin immobilized pepsin for 5-6 hours at 37°C. Undigested full antibody and Fc fragments were removed by incubation with

protein A resin. The final concentration was approximately 1μM and preparations were used directly at a 1:100 dilution.

4.5.2 Cell culture

The human breast epithelial cancer cell lines consisted of: MCF12A and MDAMB231. The MCF12A cells (ATCC, Manassas, VA) were cultured in DMEM/F12 supplemented with 20ng/mL epidermal growth factor, 0.01 mg/ml bovine insulin (Sigma-Aldrich, St. Louis, MO), 500ng/ml hydrocortisone (Sigma-Aldrich), 5% horse serum, and 1% penicillin/streptomycin (unless otherwise indicated, all were from Invitrogen Corp., Carlsbad, CA). The MDAMB cells (ATCC) were cultured in DMEM supplemented with 10% fetal bovine serum, 2mM L-glutamine, and 1% penicillin/streptomycin (all from Invitrogen Corp.). Prior to culturing cells on substrates, the cells were treated with 0.25% Trypsin-EDTA (Invitrogen Corp.) for several minutes, centrifuged, resuspended, counted, and then added to substrate.

4.5.3 Ligand stimulation

Epidermal growth factor (Invitrogen Corp., Carlsbad, CA) was added to reduced serum cells 0-48 hours prior to experiments at 2-20 ng/ml concentration. Ephrin-A1 supported membranes were formed as previously described (See Section 2.5.2).

4.5.4 Immunostaining

Cells were incubated on substrates in 37^{o}C, 5% CO_2 incubator for 1hour. Cells were then rinsed with ice cold 1xPBS and fixed with 4% paraformaldehyde (Sigma-Aldrich) in 1xPBS. The membrane was permeabilized with 0.1% Triton-X (EMD Chemicals, Gibbstown, NJ) in 1xPBS. Cells were blocked with 1%BSA 1xPBS at 4^{o}C overnight. The next day, cells were incubated with primary antibodies for 40 minutes in 1%BSA 1xPBS followed by secondary antibodies conjugated to Alexa dyes for 20 minutes. Between each incubation, the surface was rinsed with 1%BSA 1xPBS. The following antibodies were used: 1^{o} mouse monoclonal anti-EGFR (EMD Chemicals, Gibbstown, NJ), 1^{o} rabbit polyclonal anti-pEGFR 1173 (Abcam, San Francisco, CA), 2^{o} goat anti-mouse Alexa fluor 647 (Invitrogen Corp., Carlsbad, CA), and 2^{o} donkey anti-rabbit Alexa fluor 568 (Invitrogen Corp.). The dilution factor for all antibodies was 1:100.

4.5.5 Optical microscopy

TIRF microscopy was performed with a custom-built laser source as previously described.[46] To prevent overlapping emission signals, 3-color TIRF was achieved with 3 different lasers: 488nm (Coherent Inc., Santa Clara, CA), 561nm (Crystalaser, Reno, NV), and 643nm (Crystalaser, Reno, NV). A T_i Eclipse microscope was used with an inverted TIRF 100X/1.49 NA oil objective (Nikon, Burlingame, CA). Images were acquired with an EM-CCD camera (Andor Inc., South Windsor, CT) using Metamorph software.

4.5.6 Data analysis

Areas occupied by cells were chosen using cells in RICM. These same areas were designated as regions of interest in ImageJ and cropped for further analysis. To measure intensity within

ephrin-A1 clusters, first, in the RICM channel, ROIs were selected for cells that were well separated from each other. Clusters were defined as areas with 25% of the intensity of the maximum of the image in the ephrin-A1 channel. Masks were created from these clusters and the intensity for the other channels were analyzed only in these masks.

Chapter 5

Concluding Remarks

"Piled Higher and Deeper" by Jorge Cham, www.phdcomics.com

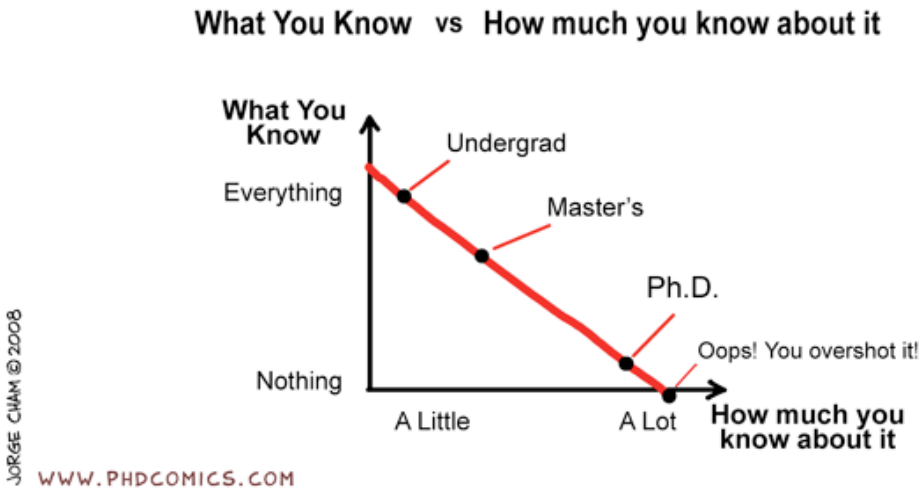

In this dissertation, I have demonstrated that an interdisciplinary approach to biological systems can yield interesting findings. In the second chapter, using synthetic chemistry to anchor monomeric ephrin-A1 to a supported membrane in a well-controlled, properly oriented manner, I showed that EphA2 can be activated in breast cancer cells. This becomes an effective and tunable platform for my later studies. In the third chapter, I combine nanotechnology with this platform to tease out an important property that is relevant to the problem of cancer metastasis related to the formation of ligand-independent EphA2 clusters. In the fourth chapter, I will be using DNA nanotechnology to enforce order on the single molecular scale. This kind of order is alluded to in bispecific antibody drug creations, currently ongoing, to target metastasis in cancer patients. Although the antibodies will block the receptors, they will also bring receptors together. This effect alone may be of significant consequences. In this dissertation, I characterized breast epithelial cells from the point of view of the EphA2 receptor on the cell membrane by spatio-mechanically altering the ephrin-A1 presentation.

Chapter 6

References

"Piled Higher and Deeper" by Jorge Cham, www.phdcomics.com

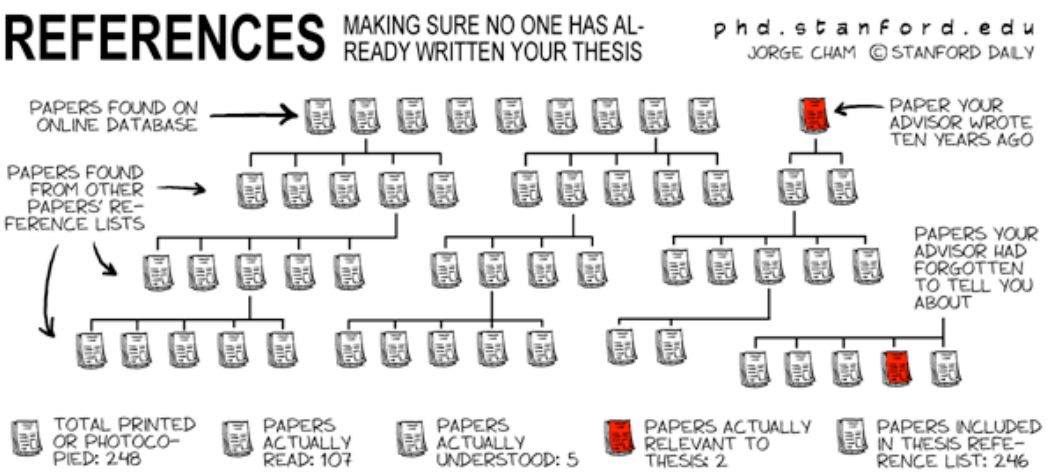

[1] Gupta, G. P. and Massague, J., Cancer metastasis: building a framework. *Cell* **127** (4), 679 (2006).

[2] Mackay, A. et al., cDNA microarray analysis of genes associated with ERBB2 (HER2/neu) overexpression in human mammary luminal epithelial cells. *Oncogene* **22** (17), 2680 (2003).

[3] Vogel, V. and Sheetz, M., Local force and geometry sensing regulate cell functions. *Nat Rev Mol Cell Biol* **7** (4), 265 (2006); Paszek, M. J. et al., Tensional homeostasis and the malignant phenotype. *Cancer Cell* **8** (3), 241 (2005).

[4] Groves, Jay T and Kuriyan, John, Molecular mechanisms in signal transduction at the membrane. *Nat Struct Mol Biol* **17** (6), 659 (2010).

[5] Lackmann, M. and Boyd, A. W., Eph, a protein family coming of age: more confusion, insight, or complexity? *Sci Signal* **1** (15), re2 (2008).

[6] Mosch, B., Reissenweber, B., Neuber, C., and Pietzsch, J., Eph receptors and ephrin ligands: important players in angiogenesis and tumor angiogenesis. *J Oncol* **2010**, 135285.

[7] Wykosky, J. and Debinski, W., The EphA2 receptor and ephrinA1 ligand in solid tumors: function and therapeutic targeting. *Mol Cancer Res* **6** (12), 1795 (2008).

[8] Kinch, M. S. and Carles-Kinch, K., Overexpression and functional alterations of the EphA2 tyrosine kinase in cancer. *Clin Exp Metastasis* **20** (1), 59 (2003); Zelinski, D. P. et al., EphA2 overexpression causes tumorigenesis of mammary epithelial cells. *Cancer Res* **61** (5), 2301 (2001).

[9] Carles-Kinch, K., Kilpatrick, K. E., Stewart, J. C., and Kinch, M. S., Antibody targeting of the EphA2 tyrosine kinase inhibits malignant cell behavior. *Cancer Res* **62** (10), 2840 (2002).

[10] Guo, H. et al., Disruption of EphA2 receptor tyrosine kinase leads to increased susceptibility to carcinogenesis in mouse skin. *Cancer Res* **66** (14), 7050 (2006).

[11] Himanen, J. P. et al., Crystal structure of an Eph receptor-ephrin complex. *Nature* **414** (6866), 933 (2001).

[12] Schlessinger, J., Cell signaling by receptor tyrosine kinases. *Cell* **103** (2), 211 (2000).

[13] Janes, P. W. et al., Adam meets Eph: an ADAM substrate recognition module acts as a molecular switch for ephrin cleavage in trans. *Cell* **123** (2), 291 (2005).

[14] Smith, F. M. et al., Dissecting the EphA3/Ephrin-A5 interactions using a novel functional mutagenesis screen. *J Biol Chem* **279** (10), 9522 (2004).

[15] Salaita, K. et al., Restriction of receptor movement alters cellular response: physical force sensing by EphA2. *Science* **327** (5971), 1380.

[16] Zhuang, G., Hunter, S., Hwang, Y., and Chen, J., Regulation of EphA2 receptor endocytosis by SHIP2 lipid phosphatase via phosphatidylinositol 3-Kinase-dependent Rac1 activation. *J Biol Chem* **282** (4), 2683 (2007).

[17] Himanen, J. P. et al., Architecture of Eph receptor clusters. *Proc Natl Acad Sci U S A* **107** (24), 10860.

[18] Grakoui, A. et al., The immunological synapse: a molecular machine controlling T cell activation. *Science* **285** (5425), 221 (1999); Manz, B. N. and Groves, J. T., Spatial organization and signal transduction at intercellular junctions. *Nat Rev Mol Cell Biol* **11** (5), 342; DeMond, A. L. et al., T cell receptor microcluster transport through molecular mazes reveals mechanism of translocation. *Biophys J* **94** (8), 3286 (2008).

[19] Mossman, K. D., Campi, G., Groves, J. T., and Dustin, M. L., Altered TCR signaling from geometrically repatterned immunological synapses. *Science* **310** (5751), 1191 (2005).

[20] Sackmann, E., Supported membranes: scientific and practical applications. *Science* **271** (5245), 43 (1996); Richter, R. P., Berat, R., and Brisson, A. R., Formation of solid-supported lipid bilayers: an integrated view. *Langmuir* **22** (8), 3497 (2006).

[21] Machan, R. and Hof, M., Lipid diffusion in planar membranes investigated by fluorescence correlation spectroscopy. *Biochim Biophys Acta* **1798** (7), 1377; Groves, J. T., Ulman, N., and Boxer, S. G., Micropatterning fluid lipid bilayers on solid supports. *Science* **275** (5300), 651 (1997).

[22] Groves, J. T., Wulfing, C., and Boxer, S. G., Electrical manipulation of glycan-phosphatidyl inositol-tethered proteins in planar supported bilayers. *Biophys J* **71** (5), 2716 (1996).

[23] Groves, J. T. and Dustin, M. L., Supported planar bilayers in studies on immune cell adhesion and communication. *J Immunol Methods* **278** (1-2), 19 (2003).

[24] Nye, J. A. and Groves, J. T., Kinetic control of histidine-tagged protein surface density on supported lipid bilayers. *Langmuir* **24** (8), 4145 (2008).

[25] Lackmann, M. et al., Ligand for EPH-related kinase (LERK) 7 is the preferred high affinity ligand for the HEK receptor. *J Biol Chem* **272** (26), 16521 (1997).

[26] Davis, S. et al., Ligands for EPH-related receptor tyrosine kinases that require membrane attachment or clustering for activity. *Science* **266** (5186), 816 (1994).

[27] Wykosky, J. et al., Soluble monomeric EphrinA1 is released from tumor cells and is a functional ligand for the EphA2 receptor. *Oncogene* **27** (58), 7260 (2008).

[28] Boniface, J. J. et al., Initiation of signal transduction through the T cell receptor requires the multivalent engagement of peptide/MHC ligands [corrected]. *Immunity* **9** (4), 459 (1998).

[29] Baksh, M. M. et al., Neuronal activation by GPI-linked neuroligin-1 displayed in synthetic lipid bilayer membranes. *Langmuir* **21** (23), 10693 (2005).

[30] Groves, J. T., Parthasarathy, R., and Forstner, M. B., Fluorescence imaging of membrane dynamics. *Annu Rev Biomed Eng* **10**, 311 (2008).

[31] Lakowicz, Joseph R., *Topics in fluorescence spectroscopy*. (Plenum Press, New York, 1991).

[32] Moran, U., Phillips, R., and Milo, R., SnapShot: key numbers in biology. *Cell* **141** (7), 1262.

[33] Meseth, U., Wohland, T., Rigler, R., and Vogel, H., Resolution of fluorescence correlation measurements. *Biophys J* **76** (3), 1619 (1999).

[34] Saffman, P. G. and Delbruck, M., Brownian motion in biological membranes. *Proc Natl Acad Sci U S A* **72** (8), 3111 (1975).

[35] Naji, A., Levine, A. J., and Pincus, P. A., Corrections to the Saffman-Delbruck mobility for membrane bound proteins. *Biophys J* **93** (11), L49 (2007).

[36] Chen, Y., Muller, J. D., So, P. T., and Gratton, E., The photon counting histogram in fluorescence fluctuation spectroscopy. *Biophys J* **77** (1), 553 (1999).

[37] Galush, W. J., Nye, J. A., and Groves, J. T., Quantitative fluorescence microscopy using supported lipid bilayer standards. *Biophys J* **95** (5), 2512 (2008).

[38] Muller, J. D., Chen, Y., and Gratton, E., Resolving heterogeneity on the single molecular level with the photon-counting histogram. *Biophys J* **78** (1), 474 (2000).

[39] Vacklin, H. P., Tiberg, F., and Thomas, R. K., Formation of supported phospholipid bilayers via co-adsorption with beta-D-dodecyl maltoside. *Biochim Biophys Acta* **1668** (1), 17 (2005).

[40] Neve, R. M. et al., A collection of breast cancer cell lines for the study of functionally distinct cancer subtypes. *Cancer Cell* **10** (6), 515 (2006).

[41] Murphy, R. M. et al., Size and structure of antigen-antibody complexes. Electron microscopy and light scattering studies. *Biophys J* **54** (1), 45 (1988).

[42] Nievergall, E. et al., PTP1B regulates Eph receptor function and trafficking. *J Cell Biol* **191** (6), 1189.

[43] Symons, M. and Segall, J. E., Rac and Rho driving tumor invasion: who's at the wheel? *Genome Biol* **10** (3), 213 (2009).

[44] Lin, W.-C., Yu, C.-H., Triffo, S., and Groves, J., Supported Membrane Formation, Characterization, Functionalization, and Patterning for Application in Biological Science and Technology. *Current Protocols in Chemical Biology*, 35 (2010).

[45] Haustein, E. and Schwille, P., Fluorescence correlation spectroscopy: novel variations of an established technique. *Annu Rev Biophys Biomol Struct* **36**, 151 (2007).

[46] Smith, A. W., Smoligovets, A. A., and Groves, J. T., Patterned Two-Photon Photoactivation Illuminates Spatial Reorganization in Live Cells. *J Phys Chem A*.

[47] Bolte, S. and Cordelieres, F. P., A guided tour into subcellular colocalization analysis in light microscopy. *J Microsc* **224** (Pt 3), 213 (2006).

[48] Middleton, E. R. and Rhoades, E., Effects of curvature and composition on alpha-synuclein binding to lipid vesicles. *Biophys J* **99** (7), 2279.

[49] Pasquale, Elena B, Eph receptor signalling casts a wide net on cell behaviour. *Nat Rev Mol Cell Biol* **6** (6), 462 (2005); Wimmer-Kleikamp, S. H. and Lackmann, M., Eph-modulated cell morphology, adhesion and motility in carcinogenesis. *IUBMB Life* **57** (6), 421 (2005).

[50] Dodelet, V. C. and Pasquale, E. B., Eph receptors and ephrin ligands: embryogenesis to tumorigenesis. *Oncogene* **19** (49), 5614 (2000).

[51] Jackson, D. et al., A human antibody-drug conjugate targeting EphA2 inhibits tumor growth in vivo. *Cancer Res* **68** (22), 9367 (2008); Hammond, S. A. et al., Selective

targeting and potent control of tumor growth using an EphA2/CD3-Bispecific single-chain antibody construct. *Cancer Res* **67** (8), 3927 (2007).

[52] Salaita, Khalid et al., Restriction of receptor movement alters cellular response: physical force sensing by EphA2. *Science* **327** (5971), 1380 (2010).

[53] Xu, Qian, Lin, Wan-Chen, Petit, Rebecca S., and Groves, Jay T., EphA2 Receptor Activation by Monomeric Ephrin-A1 On Supported Membranes. (2011).

[54] Lomüller, Theobald et al., Combining nanoparticles with supported lipid membranes: a functional static/dynamic hybrid interface for biological applications. (2011).

[55] Lomüller, Theobald et al., Nanopatterning by block copolymer micelle nanolithography and bioinspired applications. *Biointerphases* **6** (1) (2011).

[56] Seiradake, E. et al., An extracellular steric seeding mechanism for Eph-ephrin signaling platform assembly. *Nat Struct Mol Biol* **17** (4), 398; Lackmann, M. et al., Distinct subdomains of the EphA3 receptor mediate ligand binding and receptor dimerization. *J Biol Chem* **273** (32), 20228 (1998); Mudali, S. V. et al., Patterns of EphA2 protein expression in primary and metastatic pancreatic carcinoma and correlation with genetic status. *Clin Exp Metastasis* **23** (7-8), 357 (2006).

[57] Zhang, H. et al., ErbB receptors: from oncogenes to targeted cancer therapies. *J Clin Invest* **117** (8), 2051 (2007).

[58] Larsen, A. B. et al., Activation of the EGFR gene target EphA2 inhibits epidermal growth factor-induced cancer cell motility. *Mol Cancer Res* **5** (3), 283 (2007); Larsen, A. B., Stockhausen, M. T., and Poulsen, H. S., Cell adhesion and EGFR activation regulate EphA2 expression in cancer. *Cell Signal* **22** (4), 636.

[59] Van Cutsem, E. et al., Cetuximab and chemotherapy as initial treatment for metastatic colorectal cancer. *N Engl J Med* **360** (14), 1408 (2009).

[60] Krall, J. A., Beyer, E. M., and MacBeath, G., High- and low-affinity epidermal growth factor receptor-ligand interactions activate distinct signaling pathways. *PLoS One* **6** (1), e15945.

[61] Zhang, X. et al., An allosteric mechanism for activation of the kinase domain of epidermal growth factor receptor. *Cell* **125** (6), 1137 (2006).

[62] Ono, M. and Kuwano, M., Molecular mechanisms of epidermal growth factor receptor (EGFR) activation and response to gefitinib and other EGFR-targeting drugs. *Clin Cancer Res* **12** (24), 7242 (2006).

[63] Chung, I. et al., Spatial control of EGF receptor activation by reversible dimerization on living cells. *Nature* **464** (7289), 783.